

UNCLASSIFIED

Security Classification

AD 740586

DOCUMENT CONTROL DATA - R & D

(Security classification of title, body of abstract and indexing annotation must be entered when the overall report is classified)

1. ORIGINATING ACTIVITY (Corporate author) Syracuse University Syracuse, New York		7a. REPORT SECURITY CLASSIFICATION UNCLASSIFIED	
		2b. GROUP	
3. REPORT TITLE Use of the Cepstrum for Processing Multipath Signals.			
4. DESCRIPTIVE NOTES (Type of report and inclusive dates) Interim 15 Sep 1970 - 31 Dec 1971			
5. AUTHOR(S) (First name, middle initial, last name) Dr. Harry Schwarzlander			
6. REPORT DATE March 1972	7a. TOTAL NO. OF PAGES 63	7b. NO. OF REFS 10	
8a. CONTRACT OR GRANT NO. F30602-70-C-0060	8b. ORIGINATOR'S REPORT NUMBER(S)		
8c. PROJECT NO. 0171	8d. OTHER REPORT NO(S) (Any other numbers that may be assigned this report) RADC-TR-72-44		
8e. Task 01 Work Unit 003			
10. DISTRIBUTION STATEMENT Approved for public release; distribution unlimited.			
11. SUPPLEMENTARY NOTES DC-70-5		12. SPONSORING MILITARY ACTIVITY Rome Air Development Center (AFSC) (COAD) Griffiss AFB, NY 13440	
13. ABSTRACT This report summarizes a study of the use of homomorphic filtering and cepstrum analysis for processing of communications signals which have been corrupted by multipath effects. The primary objective consisted of the development of computer programs by means of which simulated multipath signals, or actual received signals after conversion to digital form - can be processed so as to reduce or eliminate the distorting effect of multipath. This objective has been met for simple discrete multipath. Extensions to more complicated multipath structures are possible. Test results have been obtained using synthesized signal sequences that simulate actual communication signals of a particular type, namely, 16-channel PSK signals as they would be generated by an HF data modem. These test results demonstrate that multipath characteristics can be identified with reasonable accuracy, for a wide range of multipath parameter values, and multipath distortion can therefore be reduced significantly. Possible practical implementations are discussed. These deviate from homomorphic filtering but utilize the cepstrum as a means for identifying the multipath structure.			

UNCLASSIFIED

Security Classification

14 KEY WORDS	LINK A		LINK B		LINK C	
	ROLE	WT	ROLE	WT	ROLE	WT
Radio Communication Systems Data Transmission Systems Multipath Transmission						

SAC--Griffiss AFB NY

UNCLASSIFIED

Security Classification

FOREWORD

This project was performed under Contract F30602-70-C-0060 by Syracuse University, Syracuse, New York. This project was supported by the Laboratory Directors Fund, Job Order Number 01717005, Task 01, Work Unit 003.

Work was performed by Dr. Harry Schwarzlander of Syracuse University (Department of Electrical Engineering) under the Post-Doctoral Program. Dr. Schwarzlander worked under the direction of Capt Brian M. Hendrickson, RADC (COAD), Project Engineer.

The Post-Doctoral Program under the direction of Dr W. W. Everett, Jr is a cooperative venture between Rome Air Development Center and various participating universities. The Post-Doctoral program provides in a contract, the opportunity for university faculty members to spend a year full time on exploratory development efforts splitting their time between RADC and the educational institutions.

This report presents interim results of computer analysis of the usefulness of cepstral techniques in reducing the effects of multipath distortion. Computer results were obtained using the RADC GE 645 Computer.

This technical report has been reviewed by the Office of Information (OI) and is releasable to the National Technical Information Service (NTIS).

This technical report has been reviewed and is approved.

Approved: *John D. Kelly*
GEORGE E. BRUNETTI
Chief, Comm Applications Branch
Communications & Navigation Div

Approved: *Frank J. Pyron*
ALVIN TWITCHELL, Colonel, USAF
Chief, Communications & Navigation Division

ABSTRACT

This report summarizes a study of the use of homomorphic filtering and cepstrum analysis for processing of communication signals which have been corrupted by multipath effects. The primary objective consisted of the development of computer programs by means of which simulated multipath signals, or actual received signals after conversion to digital form - can be processed so as to reduce or eliminate the distorting effect of multipath. This objective has been met for simple discrete multipath. Extensions to more complicated multipath structures are possible. Test results have been obtained using synthesized signal sequences that simulate actual communication signals of a particular type, namely, 16-channel PSK signals as they would be generated by an HF data modem. These test results demonstrate that multipath characteristics can be identified with reasonable accuracy, for a wide range of multipath parameter values, and multipath distortion can therefore be reduced significantly. Possible practical implementations are discussed. These deviate from homomorphic filtering but utilize the cepstrum as a means for identifying the multipath structure.

TABLE OF CONTENTS

	<u>Page</u>
1. INTRODUCTION	1
2. HOMOMORPHIC FILTERING AND THE CEPSTRUM	3
2.1 The Logarithmic Power Spectrum	3
2.2 Homomorphic Deconvolution	6
2.3 More Complicated Multipath Structure	9
2.4 Additive Noise or Interfering Signal	10
3. DISCRETE, FINITE DURATION CEPSTRAL ANALYSIS	12
3.1 The Discrete Cepstrum	12
3.2 The Multipath Cepstrum - Simplest Case	14
3.3 Multipath Cepstrum - Delay is not an integral number of sampling intervals	16
3.4 Multipath Cepstrum - Arbitrary Signal	19
3.5 Additive Noise	20
3.6 Treatment of the Errors Described in Sec. 3.4 as Additive Noise	22
3.7 Use of a Data Window	24
4. THE PSK SIGNAL	25
4.1 Specification of the PSK Signal	25
4.2 The Synthesized Signal	26
4.3 Cepstrum of the PSK Signal	26
5. THE COMPUTER PROGRAM	31
5.1 General Description	31
5.2 Data Files	33
5.3 The Main Program and Subroutines	34
5.3.1 Subroutine FFT - Fast Fourier Transform	36
5.3.2 Subroutine CLOG - Complex Logarithm	37
5.3.3 Subroutine CALOG - Antilogarithm	37
5.3.4 Subroutine SPLT - Plot Routine Driver	38
5.3.5 Subroutine SPLOT - Plot	39
5.3.6 Subroutine GEN - Data Generator	39

5.3.7	Subroutine STAT - Statistics Collector	39
5.3.8	Subroutine DET - Multipath Detection	40
5.4	Running the Program	43
6.	SYSTEM PERFORMANCE	44
6.1	Detectability of the Multipath Cepstrum	44
6.2	Effect of Error in Estimating the Magnitude of the Multipath Component	46
6.3	Extraction of Multipath Information	53
6.4	Reconstruction of Transmitted Signal Component	55
7.	DISCUSSION	56
7.1	Possible Improvements in the Present System	56
7.2	Additional Measurements	58
7.3	Possible Simplifications of the Computer Program	59
7.4	Potential Practical Application on HF Links	61

LIST OF ILLUSTRATIONS

	<u>Page</u>
Fig. 1 Sketch of Autocorrelation Function with Echo Component	3
Fig. 2 The Functions $A(f)$ and $\ln A(f)$	5
Fig. 3 Sketch of a Typical Power Spectrum and the Corresponding Log Spectrum	5
Fig. 4 Sketch of a Typical Signal Cepstrum with Superimposed Impulse Pair Due to Delay Component	6
Fig. 5 Block Diagram of Nonlinear Processing System for Homomorphic Filtering	6
Fig. 6 Deconvolution	7
Fig. 7 The Function $1 + ae^{-j2\pi f\tau}$	8
(a) Locus in complex plane	
(b) Waveforms of real and imaginary parts	
Fig. 8 Typical Discrete Multipath Cepstrum	15
Fig. 9 Discrete Multipath Cepstrum; not a multiple of the sample spacing	19
Fig. 10 Phasor Diagram for the Function $1 + ae^{-j2\pi \frac{nr}{N}} + z(n)$	21
Fig. 11 A Signal and its Delayed Replica	22
Fig. 12 Specification of Quadrature-phase Modulation	25
Fig. 13 The First 114 Points of a typical 512-point Signal Cepstrum	27
Fig. 14 The First 114 Points of a Typical 4096-point Signal Cepstrum	27
Fig. 15 Sketch of General Trend of the Discrete Logarithmic Spectrum	28
Fig. 16 Mean Value of PSK Signal Cepstrum, When Averaged Over 9 Different Signal Samples with Independent Random Modulation (First 40 points)	29
Fig. 17 Estimated Standard Deviation at the First 40 Points for 512-Point Signal Cepstra	29
Fig. 18 Maximum Positive Deviation from Mean and Maximum Negative Deviation from Mean, for the First 40 Points of the Signal Cepstrum	30
Fig. 19 Overall Functional Block Diagram of Computer Processing System	31
Fig. 20 Main Program Flow Chart	35
Fig. 21 Simplified Flow Chart for Subroutine DET	41

Fig. 22	Multipath Detection Characteristics	47
Fig. 23	Multipath Cepstrum	48
Fig. 24	Residual Cepstrum Pattern after Imperfect Cancellation	48
	a) $\alpha > 0$ and $\alpha - \hat{\alpha} > 0$	
	b) $\alpha > 0$ and $\alpha - \hat{\alpha} < 0$	
	c) $\alpha < 0$ and $\alpha - \hat{\alpha} < 0$	
	d) $\alpha < 0$ and $\alpha - \hat{\alpha} > 0$	
Fig. 25	Tapped Delay Line Representation of Residual Error	49
Fig. 26	Improvement in Signal-to-Interference Ratio	51
Fig. 27	Output Signal-to-Interference Ratio Related to Error in the Estimated Multipath Amplitude	52
Fig. 28	Extraction of the Multipath Magnitude, for $\tau \approx 2$ ms.	
Fig. 29	Alternate Scheme for Computing the Complex Cepstrum	58
Fig. 30	Recursive Filter for Multipath Cancellation	59
Fig. 31	Simplified Versions of Computer Processor	60

1. INTRODUCTION

This report summarizes a study of the use of homomorphic filtering and cepstrum analysis as described by Oppenheim, Schafer and Stockham [1] for processing of communication signals which have been corrupted by multipath effects. The primary objective consisted of the development of computer programs by means of which simulated multipath signals, or actual received signals after conversion to digital form - can be processed so as to reduce or eliminate the distorting effect of multipath. This objective has been met for simple discrete multipath. Extensions to more complicated multipath structures are possible. Test results have been obtained using synthesized signal sequences that simulate actual communication signals of a particular type, namely, 16-channel PSK signals as they would be generated by an HF data modem. These test results demonstrate that multipath characteristics can be identified with reasonable accuracy, for a wide range of multipath parameter values, and multipath distortion can therefore be reduced significantly. Possible practical implementations are discussed. These deviate from homomorphic filtering but utilize the cepstrum as a means for identifying the multipath structure.

This report is arranged into major Sections as follows:

Section 2 - Homomorphic Filtering and the Cepstrum. The basic non-linear signal processing ideas which lead to the so-called "cepstrum" are briefly surveyed, in terms of continuous signal representation. It is shown that if two signals are convolved, their cepstra are summed. Multipath is therefore an additive phenomenon in the cepstrum.

Section 3 - Discrete, Finite-Duration Cepstral Analysis. The discussion in Section 2 in terms of continuous signals is here extended to discrete (sampled) signals which are observed over a finite observation interval. Several deviations from the continuous analysis are pointed out.

Section 4 - The PSK Signal. In this Section, the 16-channel PSK signal is described which was simulated for used in all performance tests.

Section 5 - The Computer Program. The program is described which has been evolved to investigate, detect and remove multipath effects from simulated multipath signals. Sufficient detail is presented so that the various program functions and options can be understood and the program can be run.

Section 6 - System Performance. The effect of errors in the estimates of multipath parameters on the removability of the multipath distortion is analyzed. On the basis of this analysis, estimates of system performance for simple discrete multipath are obtained, neglecting additive noise. It appears that with good reliability, multipath interference can be reduced to a 20 db signal-to-interference ratio over a wide range of multipath amplitude and delay.

Section 7 - Discussion. Possible improvements of the present system are suggested, and possible forms of practical implementation are considered. More experimental data is needed in order to arrive at adequate specifications for a practical system.

2. HOMOMORPHIC FILTERING AND THE CEPSTRUM

2.1 The Logarithmic Power Spectrum

The logarithmic spectrum was described by Bogert, Healy and Tukey [2] as an approach to the separation of echoes from a received signal. Thus, consider a received signal of the form

$$y(t) = x(t) + \alpha x(t-\tau), \quad |\alpha| \leq 1, \quad (2-1)$$

where $x(t)$ is the transmitted signal. Then it may be desired to identify the parameters of the echo, that is, α and τ ; or it may be desired to extract an undistorted version of $x(t)$.

The autocorrelation function of the (real) signal $x(t)$ is

$$R_{xx}(\xi) = \left\{ \begin{array}{l} \int_{-\infty}^{\infty} x(t) x(t+\xi) dt, \text{ finite energy case} \\ \lim_{T \rightarrow \infty} \frac{1}{2T} \int_{-T}^T x(t) x(t+\xi) dt, \text{ infinite energy case} \end{array} \right\} \quad (2-2)$$

If $R_{xx}(\xi)$ has a narrow peak and is small elsewhere, autocorrelation analysis of the received signal $y(t)$ allows determination of the echo. Expressing $R_{yy}(\xi)$ in terms of $R_{xx}(\xi)$,

$$R_{yy}(\xi) = R_{xx}(\xi) + \alpha^2 R_{xx}(\xi) + \alpha R_{xx}(\xi-\tau) + \alpha R_{xx}(\xi+\tau), \quad (2-3)$$

the magnitude of the central peak is seen to be $(1+\alpha^2) R_{xx}(0) + 2\alpha R_{xx}(\tau) \approx (1+\alpha^2) R_{xx}(0)$, and the magnitudes of the peaks at $\pm\tau$ are $\alpha R_{xx}(0) + (1+\alpha^2) R_{xx}(\tau) + \alpha R_{xx}(2\tau) \approx \alpha R_{xx}(0)$.

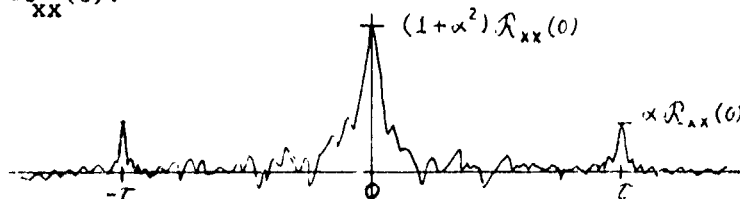


Fig. 1 Sketch of Autocorrelation Function with Echo Component

In many cases of practical interest, however, autocorrelation analysis may give inconclusive results. This is particularly true if only relatively short signal samples are available for processing.

Bogert, Healy and Tukey therefore examined the power spectrum of the received waveform in order to find a way of isolating the echo component. This led to methods of processing the received signal which involved taking the logarithm of the power spectrum. (See Table 1).

<u>Signal</u>	<u>F.T.</u>	<u>Power Spectrum</u>	<u>Log Spectrum</u>
$x(t)$	$\mathcal{F}_x(f)$	$\mathcal{G}_{xx}(f) = \mathcal{F}_x ^2$	$\mathcal{L}_{xx}(f)$
$y(t)$	$(1 + e^{-j2\pi f\tau}) \mathcal{F}_x(f)$	$A(f) \cdot \mathcal{G}_{xx}(f)$	$\ln A(f) + \mathcal{L}_{xx}(f)$

where $A(f) = (1 + \alpha^2 + 2\alpha \cos 2\pi f\tau)$

The function $A(f)$ in Table 1, and its logarithm, have the form shown in Fig. 2. In the log spectrum the nearly sinusoidal ripple of $\ln A(f)$ is superimposed on \mathcal{L}_{xx} , the log spectrum of $x(t)$. The form of \mathcal{L}_{xx} depends on $x(t)$, but some general comments can be made. Since the power spectrum generally decays toward zero with increasing $|f|$, the log spectrum goes toward large negative values with increasing $|f|$. Small ripples in \mathcal{G}_{xx} in a region where \mathcal{G}_{xx} is very small will result in very large ripples in \mathcal{L}_{xx} . Depending on the units used in computing \mathcal{G}_{xx} , it is possible that $\mathcal{G}_{xx}(f) < 1$ for all f . In that case, $\mathcal{L}_{xx}(f)$ is everywhere negative - i.e., it has a large negative "d.c. component." The latter is also present due to the negative-going trend with large $|f|$, mentioned before. A typical \mathcal{G}_{xx} and corresponding \mathcal{L}_{xx} might appear as in Fig. 3. There remains now the task of extracting the periodic ripple from \mathcal{L}_{yy} , which is basically a problem of detecting a sine-wave in the presence of noise. This can be accomplished either through autocorrelation or spectral analysis, both of which are discussed by Bogert, Healy and Tukey. Since the "signal" is now a frequency function, they speak of its cepstrum, rather than spectrum, and of its pseudo-autocovariance, rather than autocovariance. The cepstrum has been included in the continuation of Table 1. As can be seen,

<u>Log Spectrum</u>	<u>Cepstrum (Power spectrum of log spectrum)</u>
$\mathcal{L}_{xx}(f)$	$\mathcal{C}_{xx}(t')$
$\mathcal{L}_{xx}(f) + 2\alpha \cos 2\pi f\tau$	$\mathcal{C}_{xx}(t') + \alpha^2 \delta(t' - \tau) + \alpha^2 \delta(t' + \tau)$

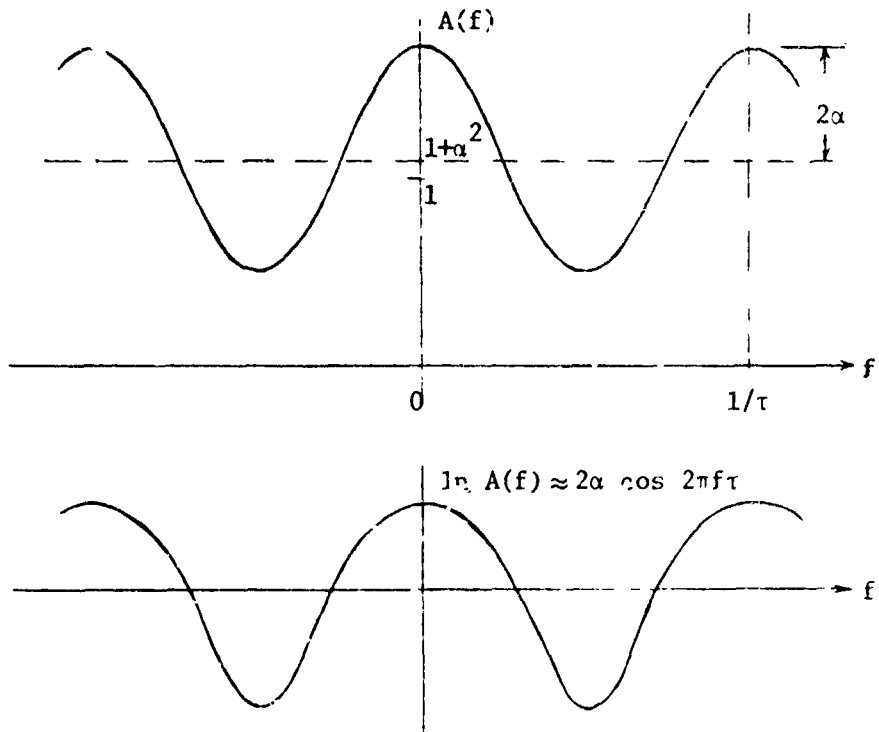


Fig. 2 The Functions $A(f)$ and $\ln A(f)$.

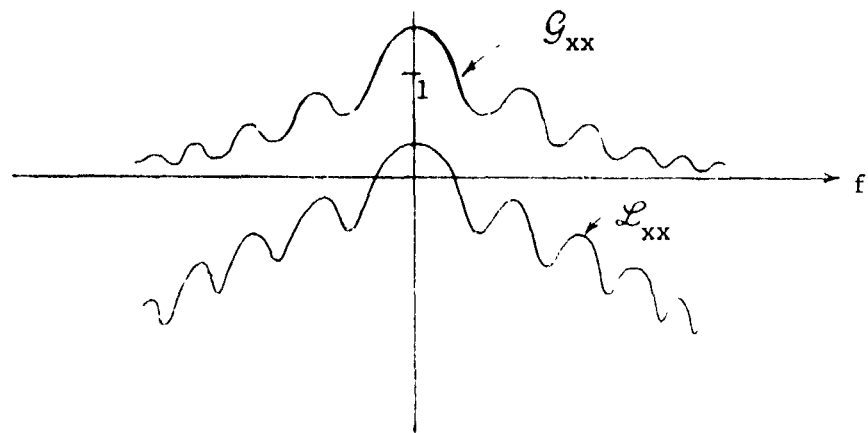


Fig. 3 Sketch of a Typical Power Spectrum and the Corresponding Log Spectrum.

the delay component in $y(t)$ has the effect of superimposing on the cepstrum of $x(t)$ a pair of impulses, located at $t' = \pm \tau$ (see Fig. 4).

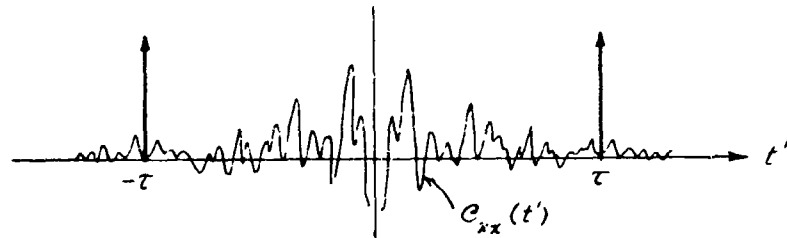


Fig. 4 Sketch of a typical signal cepstrum with superimposed impulse pair due to delay component.

Due to the fact that $\ln A(f)$ is not purely sinusoidal, there must also be small contributions at multiples of τ .

2.2 Homomorphic Deconvolution

A different approach to the identification and removal of echoes was pursued by Oppenheim, Schaffer and Stockham [1], based on the theory of homomorphic filtering developed by Oppenheim [3]. This calls for a non-linear processing system of the form shown in Fig. 5.

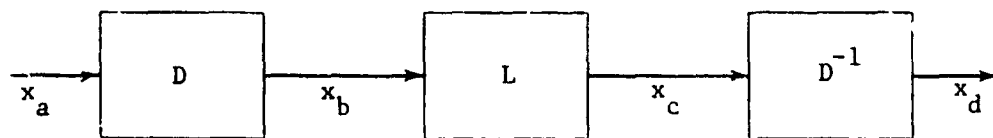


Fig. 5 Block diagram of Nonlinear Processing System for Homomorphic Filtering.

The nonlinear blocks D and D^{-1} perform homomorphic transformations of a signal space. In the application at hand, this means that D transforms a "convolutional space" into a "sum space"; that is, two signals which are convolved at the input result in images that are added. Thus, if two different signals x_{a1} , x_{a2} applies to D produce outputs x_{b1} , x_{b2} respectively, then the convolution of x_{a1} and x_{a2} , denoted $x_{a1} * x_{a2}$, produces the output $x_{b1} + x_{b2}$ (Fig. 6). This particular transformation is also called homomorphic deconvolution.

In order to accomplish homomorphic deconvolution, D must perform three operations in succession: Fourier transformation of the input signal, complex

logarithm of the resulting transform, followed by inverse Fourier transformation.

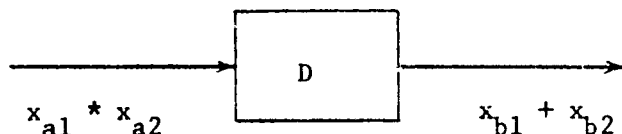


Fig. 6 Deconvolution

D^{-1} is the inverse of D . In the configuration of Fig. 5, it may then be possible to deconvolve two input signals, through linear filtering (block L in Fig. 5) and then return to the input signal space via the D^{-1} transformation.

When applied to convolved signals, homomorphic filtering becomes very similar to the generation of the cepstrum. In fact, the output obtained after the homomorphic deconvolution operation (block D in Fig. 5) may be called the complex cepstrum of the input, since the complex logarithm is involved. The details are shown in Table 2.

<u>Table 2</u>			
<u>Signal</u>	<u>F.T.</u>	<u>Complex Logarithm</u>	<u>Complex Cepstrum</u>
$x(t)$	$\mathcal{F}_x(f)$	$\mathcal{L}_x(f) = \text{cln } \mathcal{F}_x(f)$	$\mathcal{C}_x(t') = \text{inverse F.T. of } \mathcal{L}_x(f)$
$y(t)$	$(1 + \alpha e^{-j2\pi f\tau}) \mathcal{F}_x(f)$	$\text{cln}(1 + \alpha e^{-j2\pi f\tau}) + \mathcal{L}_x(f)$	see below

First it is clear that the logarithmic power spectrum of the preceding Section has a simple relation to the complex logarithm of the Fourier Transform:

$$\mathcal{L}_{xx}(f) = 2 \text{ Re } \mathcal{L}_x(f) \quad (2-4)$$

The cepstrum of Bogert, Healy and Tukey is therefore twice the even part of the complex cepstrum:

$$\mathcal{C}_{xx}(t') = 2 \text{ Ev } \mathcal{C}_x(t') \quad (2-5)$$

(For an even function, forward and inverse Fourier transforms produce the same result). Next the factor $(1+\alpha e^{-j2\pi f\tau})$ in $\mathcal{F}_y(f)$ has to be considered. The locus of this function in the complex plane is a circle centered at $1 + j0$, with radius α , so that $\text{cln}(1+\alpha e^{-j2\pi f\tau})$ has the form shown in Fig. 7.

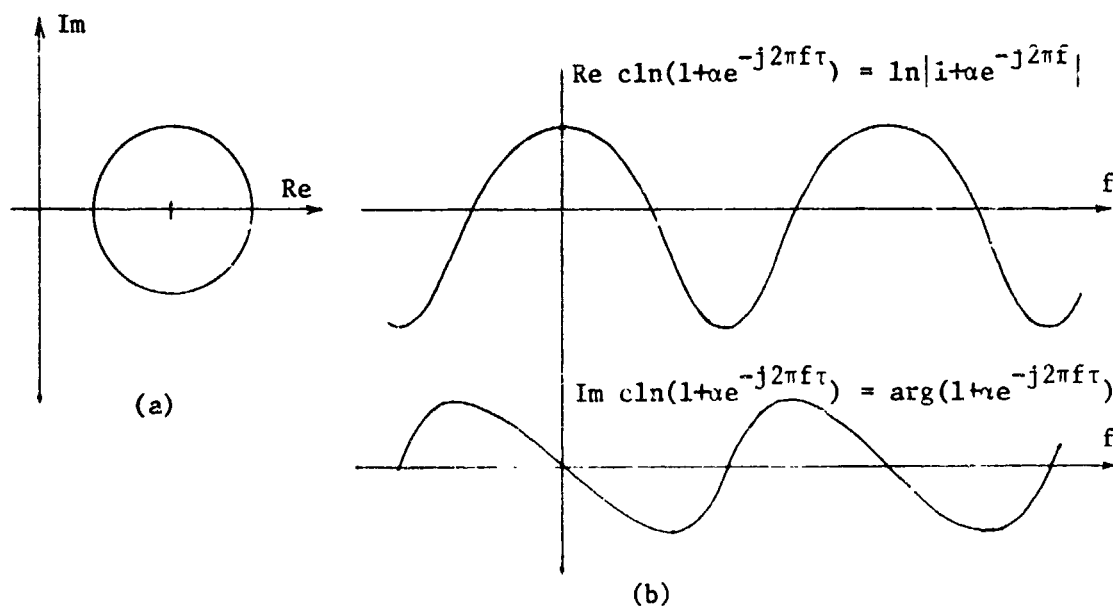


Fig. 7 The Function $1+\alpha e^{-j2\pi f\tau}$.
 (a) Locus in complex plane
 (b) Waveforms of real and imaginary parts.

These approximately sinusoidal ripples are the effect of the echo and are superimposed on the real and imaginary parts of $\mathcal{L}_x(f)$. The complex cepstrum of $y(t)$ is therefore of the form

$$\mathcal{C}_y(t') = \mathcal{C}_x(t') + \mathcal{F}^{-1} \text{.T. of } \text{cln}(1+\alpha e^{-j2\pi f\tau}). \quad (2-6)$$

Since $\text{cln}(1+\alpha e^{-j2\pi f\tau})$ is a periodic waveform, its inverse transform consists of spikes at the fundamental and harmonics (on the t' -axis). Coefficients of the impulses appearing in $\mathcal{C}_x(t')$ are obtained by expanding the logarithm:

$$\text{cln}(1+\alpha e^{-j2\pi f\tau}) = \alpha e^{-j2\pi f\tau} - \frac{\alpha^2}{2} e^{-j4\pi f\tau} + \frac{\alpha^3}{3} e^{-j6\pi f\tau} - \dots \quad (2-7)$$

The inverse transform then results in

$$\alpha\delta(t'-\tau) - \frac{\alpha^2}{2}\delta(t'-2\tau) + \frac{\alpha^3}{3}\delta(t'-3\tau) - \dots \quad (2-8)$$

Representative coefficient values are shown in Table 3.

Table 3

α	Coefficients of (2-8)			
.1	.1 ,	.005,	.00033,
.5	.5 ,	.125,	.042,
.9	.9 ,	.405,	.243,
.99	.99,	.490,	.323,

Since the signal $y(t)$ in (2-1) is obtained by passing $x(t)$ through a channel with impulse response $h(t) = \delta(t) + \alpha\delta(t-\tau)$, i.e.,

$$y(t) = x(t) * [\delta(t) + \alpha\delta(t-\tau)],$$

the expression (2-8) represents $\mathcal{C}_h(t')$, the complex cepstrum of $h(t)$. a comb filter might now be used to eliminate $\mathcal{C}_h(t')$ from $\mathcal{C}_y(t')$, leaving a relatively undistorted version of $\mathcal{C}_x(t')$. Application of the D^{-1} operation should then yield the reconstructed signal $x(t)$.

2.3 More Complicated Multipath Structure

If the received signal $y(t)$ is of a different form than has been assumed so far, the situation is considerably more complicated.

In the case of two delay components, the following expressions apply:

$$y(t) = x(t) + \alpha x(t-\tau_1) + \beta x(t-\tau_2) , \quad (2-9)$$

$$\mathcal{F}_y(f) = (1 + \alpha e^{-j2\pi f\tau_1} + \beta e^{-j2\pi f\tau_2}) \mathcal{F}_x(f) \quad (2-10)$$

$$\mathcal{L}_y(f) = \text{cln}(1 + \alpha e^{-j2\pi f\tau_1} + \beta e^{-j2\pi f\tau_2}) + \mathcal{L}_x(f) \quad (2-11)$$

Here the nature of the complex cepstrum can be inferred without resorting to detailed calculations. If the effect of the complex logarithm in (2-11) is neglected and merely the inverse transform of the term

$(1 + \alpha e^{-j2\pi f\tau_1} + \beta e^{-j2\pi f\tau_2})$ is taken, this would introduce in $\mathcal{C}_y(t')$ the impulses $\delta(t') + \alpha\delta(t' - \tau_1) + \beta\delta(t' - \tau_2)$. Due to the non-linearity of the logarithm, however, harmonics and intermodulation terms are produced. Thus, the second-order contributions appear at $2\tau_1$, $2\tau_2$, and $\tau_1 + \tau_2$. More specifically (2-7) is now replaced by:

$$\begin{aligned} \text{cIn}(1 + \alpha e^{-j2\pi f\tau_1} + \beta e^{-j2\pi f\tau_2}) &= (\alpha e^{-j2\pi f\tau_1} + \beta e^{-j2\pi f\tau_2}) \\ &- \frac{1}{2} (\alpha^2 e^{-j4\pi f\tau_1} + 2\alpha\beta e^{-j2\pi f(\tau_1 + \tau_2)} + \beta^2 e^{-j4\pi f\tau_2}) \\ &+ \dots \end{aligned} \quad (2-12)$$

It is easy to identify from this expansion the coefficients and locations of all those impulses in $\mathcal{C}_y(t')$ which are due to the delay structure.

2.4 Additive Noise or Interfering Signal

As soon as an additive interference is specified, the analysis becomes more complicated. Consider low-level noise, $v(t)$, superimposed on the multipath signal:

$$x(t) + \alpha x(t - \tau) + v(t) \quad (2-13)$$

In the frequency domain this becomes

$$\mathcal{F}_x(f) (1 + \alpha e^{-j2\pi f\tau}) + \mathcal{F}_v(f) \quad (2-14)$$

which can be written

$$\mathcal{F}_x(f) \left[1 + \alpha e^{-j2\pi f\tau} + \frac{\mathcal{F}_v(f)}{\mathcal{F}_x(f)} \right] \quad (2-15)$$

The complex cepstrum is

$$\mathcal{C}_x(t') + \text{F.T.}^{-1} \text{ of } \text{cIn} \left[1 + \alpha e^{-j2\pi f\tau} + \frac{\mathcal{F}_v(f)}{\mathcal{F}_x(f)} \right] \quad (2-16)$$

The term $\frac{\mathcal{F}_y(f)}{\mathcal{F}_x(f)}$ in effect represents a random phase and amplitude modulation of $\alpha e^{-j2\pi f\tau}$. This modulation appears in the cepstrum domain in the form of noise sidebands about the spike pattern which identifies the multipath characteristics. The spike pattern itself is not affected, however, as long as infinite-time, continuous analysis is used. Acceptable behavior of $\mathcal{F}_x(f)$ is also assumed.

3. DISCRETE, FINITE DURATION CEPSTRAL ANALYSIS

When working with finite duration sample sequences, as is the case when using "Fast Fourier Transform" (FFT) techniques, the analysis of the previous chapter is not directly applicable. Some of the differences will be explained in this chapter.

3.1 The Discrete Cepstrum

In Table 4, a comparison between the continuous and discrete finite-duration cepstral analysis is drawn up. (Braces denote sequences of numbers.)

	<u>continuous</u>	<u>discrete</u>
The signal	$x(t), -\infty < t < \infty$	$\{x_k\} k = 0, \dots, N-1$ where the k^{th} sample value $x_k = x\left(\frac{kT}{N}\right)$
The spectrum	$\mathcal{F}_x(f)$	$\{d_x(n)\} = \left\{ \frac{1}{N} \sum_{k=0}^{N-1} x_k e^{-j\frac{2\pi nk}{N}} \right\},$ $n = 0, \dots, N-1.$
The log spectrum	$\mathcal{L}_x(f)$	$\{\ell_x(n)\} = \text{cln}\{d_x(n)\}$
The complex cepstrum	$\mathcal{C}_x(t')$	$\{c_x(k)\} = \left\{ \sum_{n=0}^{N-1} \ell_x(n) e^{j\frac{2\pi nk}{N}} \right\} k=0, \dots, N-1$

The discrete spectrum $\{d_x(n)\}$ in general is not just a sampled version of $\mathcal{F}_x(f)$, but includes an aliasing effect, (if $x(t)$ is not bandlimited to frequencies below $\frac{N}{2T}$) and the effect of truncation in the time domain. The precise relation between sample values of \mathcal{L}_x and the sequence $\{\ell_x\}$ is

somewhat obscure, because the effects of aliasing and time-domain truncation, which are present in $\{d_x\}$, have become intermixed with the sample values of \mathcal{L}_x . The same is true for the relation between \mathcal{C}_x and $\{c_x\}$. However, these effects are small if a large record is processed, and if sampling is sufficiently rapid so that little aliasing arises. The discrepancy due to truncation in time disappears if the signal x is periodic, with period T .

Discrete cepstral analysis can also be discussed in terms of z -transforms. The z -transform representation of the signal sequence $\{x_k\}$ is defined as

$$\mathcal{Z}_x(z) = \sum_{k=0}^{N-1} x_k z^{-k}, \quad (3-1)$$

so that

$$\{d_x(n)\} = \frac{1}{N} \{ \mathcal{Z}_x(e^{j\frac{2\pi n}{N}}) \}. \quad (3-2)$$

This is a sequence of N values of $\mathcal{Z}_x(z)$ which occur at equally spaced points along the unit circle in the z -plane, multiplied by $1/N$. Then

$$\{\ell_x(n)\} = \text{cln}\{d_x(n)\} = -\ln N + \{ \text{cln} \mathcal{Z}_x(e^{j\frac{2\pi n}{N}}) \} \quad (3-3)$$

But $\text{cln} \mathcal{Z}_x$ can itself be regarded as the z -transform of some sequence. Thus, let

$$\mathcal{Z}_{c_x}(z) = -\ln N + N \text{cln} \mathcal{Z}_x(z), \quad (3-4)$$

so that $\{\ell_x(n)\} = \frac{1}{N} \{ \mathcal{Z}_{c_x}(e^{j\frac{2\pi n}{N}}) \}$. Comparison with (3-2) shows that $\{\ell_x(n)\}$ is then the DFT of the sequence of numbers whose z -transform is

$$\mathcal{Z}_{c_x}(z) = \sum_{k=0}^{N-1} c_x(k) z^{-k}. \quad \text{In other words,}$$

$\{\ell_x(n)\}$ is the DFT of the complex cepstrum $\{c_x(k)\}$.

3.2 The Multipath Cepstrum - Simplest Case

In order to see how the effect of multipath appears in the discrete cepstrum, we consider first the case of a periodic signal with period T , and a multipath delay which equals an integral number of sampling intervals. Thus, we have a transmitted signal $x(t) = x(t-T)$ and a received signal $y(t)$ as in (2-1),

$$y(t) = x(t) + \alpha(t-\tau),$$

but with

$$\tau = \frac{rT}{N}, \quad (3-5)$$

where r is any integer from 1 to $N-1$.

Since x is periodic, \mathcal{F}_x is discrete. If, in addition, x is strictly bandlimited to frequencies less than $\frac{N}{2T}$, then the coefficients of \mathcal{F}_x within the band limits coincide with $\{d_x(n)\}$ (see [10].) The assumption that x is strictly bandlimited is not needed here, however, and it will be understood that the discrete spectrum $\{d_x(n)\}$ may differ from \mathcal{F}_x .

In place of the F.T. of y (Table 2), the DFT of y is now considered:

$$\{d_y(n)\} = \{d_x(n)(1 + \alpha e^{-j2\pi\frac{nr}{N}})\}, \quad n=0,1,\dots,N-1 \quad (3-6)$$

$$\{\ell_y(n)\} = \{\ell_x(n)\} + \{c \ln(1 + \alpha e^{-j2\pi\frac{nr}{N}})\} \quad (3-7)$$

$$\{c_y(k)\} = \{c_x(k)\} + \text{DFT}^{-1}\{c \ln[1 + \alpha e^{-j2\pi\frac{nr}{N}}]\} \quad (3-8)$$

The second term in (3-8) gives, using (2-7):

$$\begin{aligned} \{c_m(k)\} &= \left\{ \sum_{n=0}^{N-1} c \ln(1 + \alpha e^{-j2\pi\frac{nr}{N}}) e^{j\frac{2\pi nk}{N}} \right\} \\ &= \left\{ \sum_{n=0}^{N-1} \left(- \sum_{p=1}^{\infty} \frac{(-\alpha)^p}{p} e^{-j2\pi p\frac{nr}{N}} \right) e^{j\frac{2\pi nk}{N}} \right\} \end{aligned}$$

$$= \left. \begin{cases} \frac{-N(-\alpha)^p}{p} & \text{for } k = pr \quad (p = 1, 2, \dots) \pmod{N}. \\ 0 & \text{otherwise} \end{cases} \right\} \quad (3-9)$$

Alternately, the sampled representation of $y(t)$ can be expressed in terms of its z-transform:

$$Z_y(z) = Z_x(z) + \alpha z^r Z_x(z) = Z_x(z)(1 + \alpha z^r). \quad (3-10)$$

Then

$$\begin{aligned} Z_{c_y}(z) &= -N \ln N + N \operatorname{cln} Z_y(z) \\ &= -N \ln N + N \operatorname{cln} Z_x(z) + N \operatorname{cln} (1 + \alpha z^r) \\ &= Z_{c_x}(z) - N \sum_{p=1}^{\infty} \frac{(-\alpha)^p}{p} z^{-rp} \end{aligned} \quad (3-11)$$

The last term is the z-transform of the multipath cepstrum $\{c_m(k)\}$, so that (3-9) is again obtained. In other words, superimposed on the discrete cepstrum $\{c_x\}$ appears a multipath pattern such as shown in Fig. 8 for the particular case $\alpha = 0.5$, $r = 5$, $N = 512$.

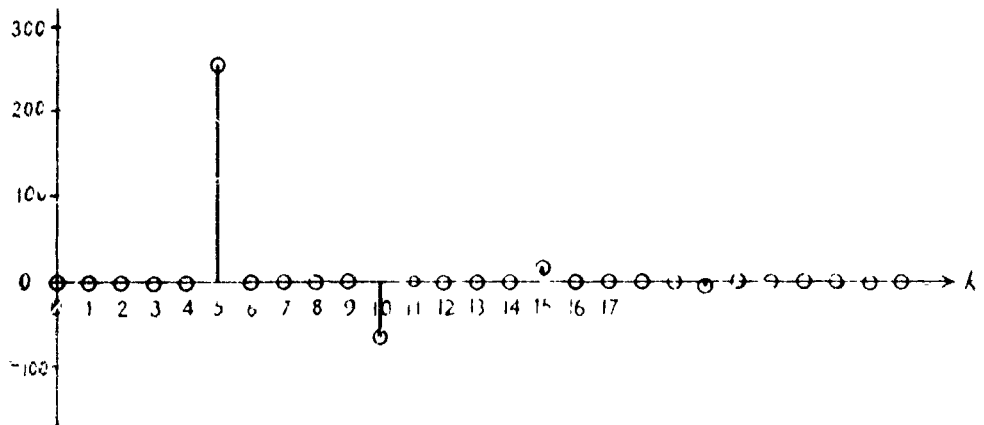


Fig. 8 Typical Discrete Multipath Cepstrum

3.3 Multipath Cepstrum - Delay is not an integral number of sampling intervals

Next, an arbitrary multipath delay τ , is considered but x still periodic with period T . Here $x(t)$ will at first be assumed bandlimited to frequencies below $\frac{N}{2T}$. The received signal is

$$y(t) = x(t) + \alpha x(t-\tau),$$

or in terms of sample values,

$$\{y_k\} = \{x_k + \alpha x_{(\tau)k}\} \quad (3-12)$$

where the $x_{(\tau)k}$ are samples of a delayed version of x (delayed by τ sec.) Since x is bandlimited, the $x_{(\tau)k}$ can be expressed exactly in terms of the x_k 's, using the sampling expansion of $x(t)$:

$$x(t) = \sum_{k=-\infty}^{\infty} x_k \operatorname{sinc} \left(\frac{Nt}{T} - k \right) \quad (\text{where } x_{k+N} = x_k, k = \dots -1, 0, 1, \dots).$$

Thus,

$$x_{(\tau)k} = x\left(\frac{T}{N}k - \tau\right) = \sum_{p=-\infty}^{\infty} x\left(\frac{T}{N}p\right) \operatorname{sinc} \left(k - \tau \frac{N}{T} - p \right). \quad (3-13)$$

Since x is taken to be periodic with period T , only N distinct coefficients are involved in (3-13), which can therefore be written in the following way in order to exhibit that fact:

$$x_{(\tau)k} = \sum_{r=-\infty}^{\infty} \sum_{p=0}^{N-1} x_p \operatorname{sinc} \left(k - \tau \frac{N}{T} - p - rN \right). \quad (3-14)$$

Application of the FFT to $x_{(\tau)k}$ gives

$$\begin{aligned} d_{x_{(\tau)}}(n) &= \frac{1}{N} \sum_{k=0}^{N-1} \sum_{p=-\infty}^{\infty} x_p \operatorname{sinc} \left(k - \tau \frac{N}{T} - p \right) e^{-j2\pi \frac{nk}{N}} \\ &= \frac{1}{N} \sum_{k=0}^{N-1} \sum_{r=-\infty}^{\infty} \sum_{p=0}^{N-1} x_p \operatorname{sinc} \left(k - \tau \frac{N}{T} - p - rN \right) e^{-j2\pi \frac{nk}{N}} \end{aligned} \quad (3-15)$$

The DFT of $\{y_k\}$ is therefore

$$\begin{aligned} d_y(\tau) &= \frac{1}{N} \sum_{k=0}^{N-1} \left[x_k + \alpha \sum_{p=-\infty}^{\infty} x_p \operatorname{sinc}\left(k - \tau \frac{N}{T} - p\right) \right] e^{-j2\pi \frac{nk}{N}} \\ &= d_x(n) + \frac{\alpha}{N} \sum_{p=-\infty}^{\infty} \sum_{k=0}^{N-1} x_p \operatorname{sinc}\left(k - \tau \frac{N}{T} - p\right) e^{-j2\pi \frac{nk}{N}} \end{aligned} \quad (3-16)$$

The second term becomes, upon replacing p by $k + \tau$:

$$\begin{aligned} &\frac{\alpha}{N} \sum_{p=-\infty}^{\infty} \sum_{k=0}^{N-1} x_{k+p} \operatorname{sinc}\left(\tau \frac{N}{T} + p\right) e^{-j2\pi \frac{nk}{N}} \\ &= \alpha d_x(n) \sum_{p=-\infty}^{\infty} \operatorname{sinc}\left(\tau \frac{N}{T} + p\right) e^{j2\pi \frac{np}{N}} ; \end{aligned}$$

so that (3-16) becomes

$$d_y(n) = d_x(n) \left[1 + \alpha \sum_{p=-\infty}^{\infty} \operatorname{sinc}\left(\tau \frac{N}{T} + p\right) e^{j2\pi \frac{np}{N}} \right]. \quad (3-17)$$

This should be compared with (3-6), to which it reduces if τ is a multiple of $\frac{T}{N}$. The discrete cepstrum then becomes

$$\begin{aligned} c_y(k) &= c_x(k) + \text{D.F.T.}^{-1} \left\{ \ln \left[1 + \alpha \sum_{p=-\infty}^{\infty} \operatorname{sinc}\left(\tau \frac{N}{T} + p\right) e^{j2\pi \frac{np}{N}} \right] \right\} \\ &= c_x(k) + \text{D.F.T.}^{-1} \left[\left(\alpha \sum_p \dots \right) - \frac{1}{2} \left(\alpha \sum_p \dots \right)^2 + \frac{1}{3} \left(\alpha \sum_p \dots \right)^3 - \dots \right] \end{aligned} \quad (3-18)$$

The first-order multipath term is, for $k = 0, 1, \dots, N-1$,

$$c_{m1}(k) = \sum_{n=0}^{N-1} \alpha \sum_{p=-\infty}^{\infty} \operatorname{sinc}\left(\tau \frac{N}{T} + p\right) e^{j2\pi \frac{np}{N}} e^{j2\pi \frac{nk}{N}}$$

$$= \alpha \sum_{p=-\infty}^{\infty} \sum_{n=0}^{N-1} \text{sinc} \left(\tau \frac{N}{T} + p \right) e^{j2\pi \frac{n(p+k)}{N}}$$

Only those terms for which $p = -k \pm mN$ are terms which contribute to the result, giving

$$c_{m1}(k) = \alpha N \sum_{m=-\infty}^{\infty} \text{sinc} \left(\tau \frac{N}{T} - k + mN \right) = \alpha \sin \pi \left(\tau \frac{N}{T} - k \right) \cot \pi \left(\frac{\tau}{T} - \frac{k}{N} \right)$$

$$\approx \alpha N \text{sinc} \left(\tau \frac{N}{T} - k \right), \text{ for } \frac{\tau}{T} - \frac{k}{N} \ll 1. \quad (3-19)$$

The second-order multipath term is, for $k = 0, 1, \dots, N-1$

$$\begin{aligned} c_{m2}(k) &= \sum_{n=0}^{N-1} \frac{\alpha^2}{2} \sum_{p=-\infty}^{\infty} \sum_{q=-\infty}^{\infty} \text{sinc} \left(\tau \frac{N}{T} + p \right) \text{sinc} \left(\tau \frac{N}{T} + q \right) e^{j2\pi \frac{n(p+q)}{N}} e^{j2\pi \frac{nk}{N}} \\ &= \frac{\alpha^2}{2} \sum_{p=-\infty}^{\infty} \sum_{q=-\infty}^{\infty} \text{sinc} \left(\tau \frac{N}{T} + p \right) \text{sinc} \left(\tau \frac{N}{T} + q \right) \sum_{n=0}^{N-1} e^{j2\pi \frac{n(p+q+k)}{N}}. \end{aligned}$$

Only those terms contribute for which $p + q = -k \pm mN$. Then

$$c_{m2}(k) = \frac{\alpha^2 N}{2} \sum_{m=-\infty}^{\infty} \sum_{q=-\infty}^{\infty} \text{sinc} \left(\tau \frac{N}{T} - k - q + mN \right) \text{sinc} \left(\tau \frac{N}{T} + q \right).$$

The inner summation is a discrete convolution of two sinc-functions which yields again a sinc-function:

$$c_{m2}(k) = \frac{\alpha^2 N}{2} \sum_{m=-\infty}^{\infty} \text{sinc} \left(2\tau \frac{N}{T} - k + mN \right) = \frac{\alpha^2}{2} \sin \pi \left(2\tau \frac{N}{T} - k \right) \cot \pi \left(\frac{2\tau}{T} - \frac{k}{N} \right)$$

$$\approx \frac{\alpha^2 N}{2} \text{sinc} \left(2\tau \frac{N}{T} - k \right), \text{ for } \frac{2\tau}{T} - \frac{k}{N} \ll 1 \quad (3-20)$$

In a similar way are the remaining multipath terms approximated by discrete sinc-functions. (3-18) therefore becomes

$$c_y(k) \approx c_x(k) - N \sum_{p=1}^{\infty} \frac{(-\alpha)^p}{p} \text{sinc}(p\tau \frac{N}{T} - k), \quad k = 0, 1, \dots, N-1 \quad (3-21)$$

The argument of the sinc-function is to be understood as mod N for each p. Thus there appears superimposed on the discrete cepstrum $\{c_x\}$ a multipath pattern such as shown in Fig. 9 for the case $\alpha = 0.5$, $\tau = 5.5 \frac{T}{N}$, $N = 512$:

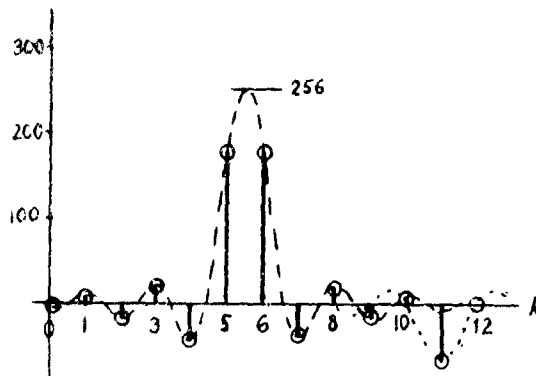


Fig. 9 Discrete Multipath Cepstrum; τ not a multiple of the sample spacing.

3.4 Multipath Cepstrum - Arbitrary Signal

For an arbitrary signal $x(t)$, two sources of error enter into expression (3-20). First, if $x(t)$ is not periodic with period T , the values $x(\frac{T}{N}k - \tau)$ (for $k = 0, 1, \dots, N-1$) are no longer expressible exactly in terms of the samples $x(k\frac{T}{N})$. Instead of (3-13), only an approximate expression can be given,

$$x_{(\tau)k} \approx \sum_{p=0}^{N-1} x(p\frac{T}{N}) \text{sinc}(k - \tau\frac{N}{T} - p), \quad (3-22)$$

where the approximation is reasonable only for $\frac{T}{N}k - \tau$ within the interval $(0, T)$, and not too close to the end points of this interval. Second, if $x(t)$ is not bandlimited to frequencies below $\frac{N}{2T}$, then an additional error is introduced due to frequency-domain aliasing.

The two effects just described are not very significant if

- a) rather long sample sequences are processed;
- b) the signal is sampled sufficiently rapidly so that a negligible fraction of signal energy lies outside the frequency range below $\frac{N}{2T}$; and
- c) the maximum multipath delay τ is much smaller than T .

Their requirements have been assumed to hold in this investigation. The multipath detection procedure described in Chapter 5 has therefore been based on Eqs. (3-9) and (3-21).

The discrete analysis extends in an analogous manner to more complicated multipath structures, such as described in Equ. (2-9) through (2-12) in terms of continuous cepstral analysis. However, the multipath detection and cancellation procedure presently programmed and described in Chapter 5 operate only on a single multipath component.

3.5 Additive Noise

Extension of Equ. (2-16) to the finite duration discrete case gives for the discrete cepstrum of a multipath signal with additive noise:

$$c_x(k) + \text{D.F.T.}^{-1} \left[c \ln \left(1 + \alpha e^{-j2\pi \frac{nr}{N}} + \frac{d_v(n)}{d_x(n)} \right) \right] \quad (3-23)$$

For convenience, multipath delay is assumed a multiple of the sampling interval, as in Sec. 3.2, and is expressed by (3-5). As in the continuous case, the term $\frac{d_v(n)}{d_x(n)}$ can be regarded as random phase and amplitude modulation of $\alpha e^{-j2\pi \frac{nr}{N}}$, which introduces noise sidebands about the multipath spikes in the discrete cepstrum. In the discrete case, however, because of the finite observation time, a random error will also appear superimposed on the magnitudes of the multipath spikes. A detailed quantitative derivation of this effect has not been carried out. However, from a first-order analysis it follows that the noise does not bias the magnitudes of the multipath spikes in the real cepstrum.

In order to show this, attention is restricted to the real logarithm in (3-23), that is,

$$\ln \left| 1 + \alpha e^{-j2\pi \frac{nr}{N}} + z(n) \right| \quad (3-24)$$

where $z(n) = d_v(n)/d_x(n)$. The phasor diagram in Fig. 10 is helpful:

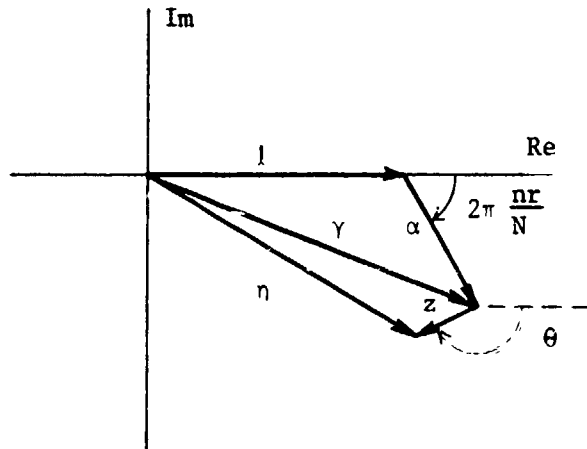


Fig. 10 Phasor diagram for the function $1 + \alpha e^{-j2\pi \frac{nr}{N}} + z(n)$

The phasor with magnitude α advances with n in discrete steps of size $\frac{2\pi r}{N}$. For given n , its sum with the unit vector has been denoted γ in Fig. 10, where

$$|\gamma| = \sqrt{1 + 2\alpha \cos 2\pi \frac{nr}{N} + \alpha^2}. \quad (3-25)$$

Only the magnitude of γ is needed since θ , the argument of the random phasor $z(n)$, is assumed uniformly distributed over $(0, 2\pi)$, and independent of $|z|$ and $\arg \gamma$. Adding to γ the random phasor z results in n , where

$$|n| = |\gamma| \sqrt{1 + 2 \left| \frac{z}{\gamma} \right| \cos \theta + \left| \frac{z}{\gamma} \right|^2} \quad (3-26)$$

In order to average out the effect of θ , the expected value with respect to θ can be computed. This can be done as follows, under the

assumption that the noise is small so that $|\frac{z}{\gamma}| < 1$ for all n :

$$E_{\theta} \ln|\eta| = E_{\theta} \left\{ \ln|\gamma| + \frac{1}{2} \ln(1 + 2|\frac{z}{\gamma}| \cos \theta + |\frac{z}{\gamma}|^2) \right\},$$

where $\frac{1}{2} \ln(1 + 2|\frac{z}{\gamma}| \cos \theta + |\frac{z}{\gamma}|^2) = \mathcal{R}e \ln(1 + |\frac{z}{\gamma}| e^{j\theta})$, so that

$$\begin{aligned} E_{\theta} \ln|\eta| &= \ln|\gamma| + E_{\theta} \left\{ |\frac{z}{\gamma}| \cos \theta - \frac{1}{2} |\frac{z}{\gamma}|^2 \cos 2\theta + \dots \right\} \\ &= \ln|\gamma|. \end{aligned} \tag{3-27}$$

The expected values of the multipath cepstrum are therefore not affected by the noise, in the case of large signal-to-noise ratio.

3.6 Treatment of the Errors Described in Sec. 3.4 as Additive Noise

If the transmitted signal is not assumed periodic with period T , then a discrepancy arises due to the fact that the observed portion of the delayed signal component, $ax(t-\tau)$, is not merely a delayed version of the observed portion of the transmitted signal component $x(t)$.

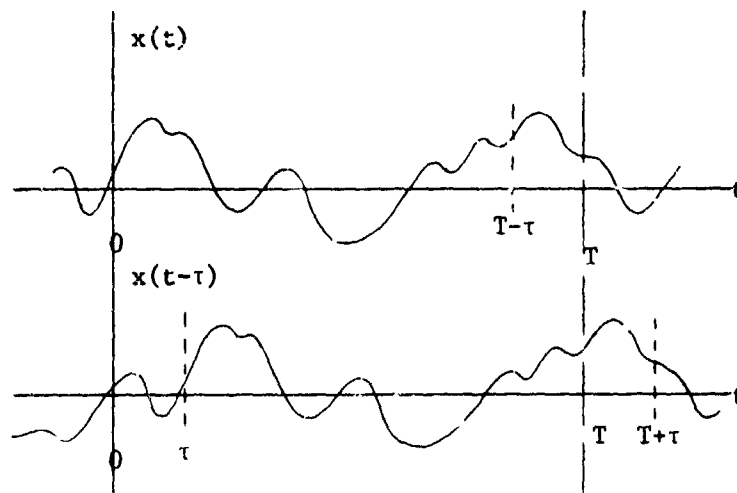


Fig. 11 A Signal and its Delayed Replica

Fig. 11 shows a signal waveform $x(t)$, and its delayed replica, $x(t-\tau)$. When observation is confined to $(0, T)$, the delayed signal as observed does not correspond to the observed portion of $x(t)$, but only to $x(t)$ within $(0, T-\tau)$. Also, in the interval $(0, -)$, the delayed waveform does not agree with the observed $x(t)$ anywhere. This can be viewed in the following way. Let

$$\left. \begin{aligned} x_0(t) &= \begin{cases} x(t), & 0 \leq t < T-\tau \\ 0, & T-\tau \leq t < T \end{cases} \\ x_1(t) &= \begin{cases} x(t), & T-\tau \leq t < T \\ 0, & 0 \leq t < T-\tau \end{cases} \\ x_{-1}(t) &= \begin{cases} x(t) & -\tau \leq t < 0 \\ 0 & \text{otherwise} \end{cases} \end{aligned} \right\} (3-28)$$

Then the observed portion of $x(t)$ can be expressed in terms of two components,

$$x(t) = x_0(t) + x_1(t) \quad (3-29)$$

The observed portion of the received multipath signal can be written

$$y(t) = x(t) + \alpha x(t-\tau) = x_0(t) + \alpha x_0(t-\tau) + x_1(t) + \alpha x_{-1}(t-\tau). \quad (3-30)$$

Within the observation interval, only the x_0 component appears to have undergone multipath delay. Therefore, when the received signal (3-30) undergoes finite-duration discrete cepstral analysis, the x_1 and x_{-1} terms can be viewed as noise which does not carry any multipath information. The signal-to-noise ratio can still be considered small, as long as $\tau \ll T$. However, the waveform segments $x_1(t)$ and $\alpha x_{-1}(t-\tau)$ are dependent (in amplitude and duration) on the multipath characteristics. Therefore, their mean effect on the multipath cepstrum is not zero, as would be the case for independent low-level

noise. Instead, the multipath cepstrum appears as an attenuated version of the ideal multipath cepstrum, with an attenuation roughly proportional to τ/T .

3.7 Use of a Data Window

The effect just described, as well as spectrum spread due to truncation of the time waveform, can be reduced by the use of a data window. Only one type of window, a "Hanning" window, has been tried. This consists of multiplying the first 26 data points, x_0, x_1, \dots, x_{25} , by $\frac{1}{2}(1 - \cos \frac{n\pi}{25})$ for $n = 0, 1, \dots, 25$, and the last 25 data points by $\frac{1}{2}(1 - \cos \frac{(N-n)\pi}{25})$ for $n = N-25, N-24, \dots, N-1$.

Because use of the window appears to strengthen the detectability of the multipath cepstrum components, this window has been included in the final version of the computer program. However, the effect of the window on the cepstrum has not yet been studied analytically, nor an optimum window shape determined.

4. THE PSK SIGNAL

The accuracy with which the multipath characteristic of a channel can be estimated depends strongly on the type of transmitted signal. The cepstra of the possible transmitted signals have to be sufficiently similar to each other, and at the same time sufficiently distinct from the class of multipath cepstra, in order to permit a reasonably accurate determination of the multipath characteristic. Of course, perfect identification of the multipath characteristic can never be assured because of the effects discussed in Sec. 3.4.

4.1 Specification of the PSK Signal

The signals which have been considered in this study are multi-channel PSK signals as they would be generated by a 16-channel HF data modem, in accordance with MIL-STD-188C. This type of signal has a structure which makes possible the extraction of useful multipath information from the cepstrum. It consists of 16 differentially coherent phase-shift keyed tones at frequencies $(935 + k \cdot 110)$ Hz (where $k = 0, 1, \dots, 15$). Keying is simultaneous in all channels, at 75 bauds per second. Fig. 12 describes the four-phase encoding which is specified:

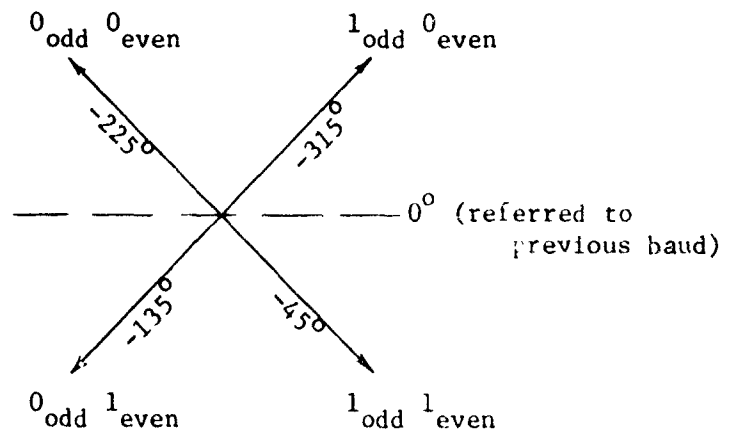


Fig. 12 Specification of Quadra-phase Modulation

A synchronizing tone at 825 Hz, which is also called for in MIL-STD-188C, and an optional 605 Hz Doppler tone, were not incorporated in the synthesized signals.

4.2 The Synthesized Signal

Sequences of signal samples, representing samples of the PSK signal as described above, were synthesized. Independent, random modulation was used on all channels. Such synthesized signal sequences were used in all tests performed with the computer program described in the next Chapter.

A sampling rate of 8,175 samples/sec. was used. This resulted in exactly 109 samples/ baud. A signal sequence of 512 samples (or 1024 samples) therefore did not consist of an integer number of bauds.

In order to minimize the frequency-domain aliasing effect it was desirable to approximate the bandlimiting effect of practical transmission channels and filters. For this reason, the synthesized signal was modified near the baud transitions by a sine-integral weighting, extending 5 samples to either side of the baud boundary. This had the same effect as approximately bandlimiting the ideal 10-channel PSK waveform to a frequency of 4.0875 kHz (the Nyquist frequency) prior to sampling.

4.3 Cepstrum of the PSK Signal

Analytic derivation of the signal cepstrum is awkward and does not lead to a closed form. Instead, the investigation has centered around computer-generated (discrete) real cepstra of the PSK signal. Examples of these are shown in Figs. 13 and 14. Only the real cepstra (inverse DFT of real logarithm of spectrum) have been used because the imaginary part of the logarithm tends to yield too irregular a cepstrum. The latter therefore has so far not been utilized for multipath detection. This has the disadvantage that the polarity of the multipath delay

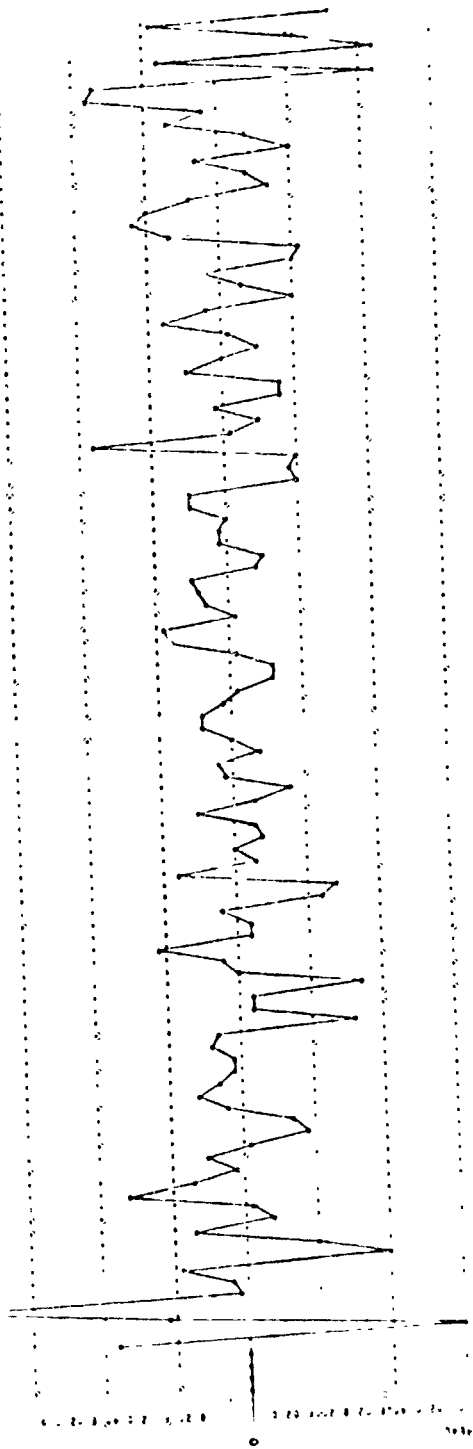


Fig. 13 The first 114 points of a typical 512-point signal cepstrum

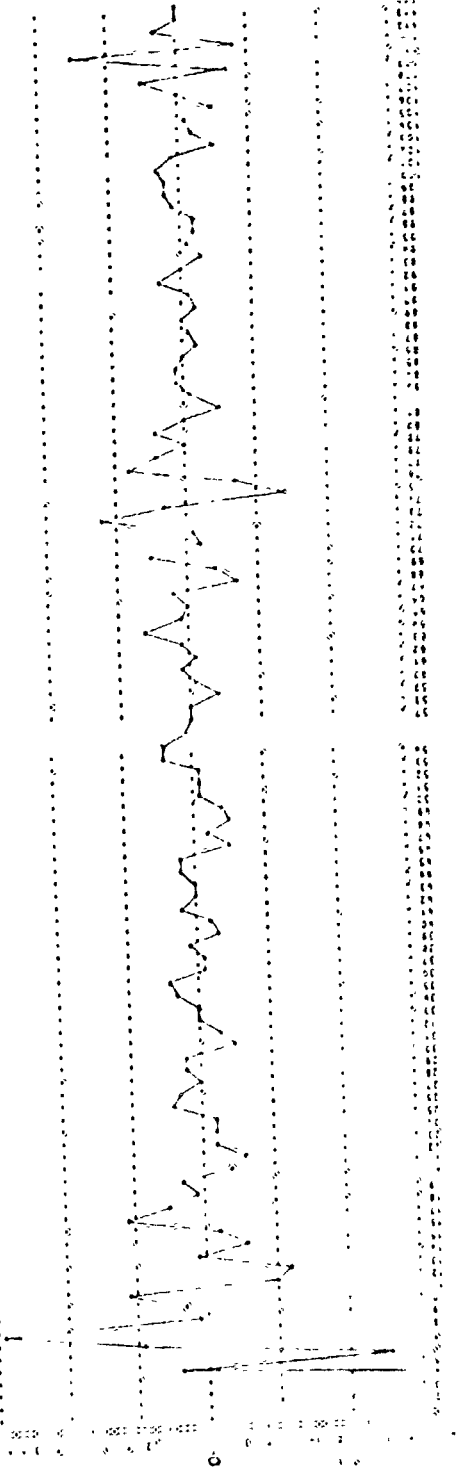


Fig. 14 The first 114 points of a typical 4096-point signal cepstrum

is lost. The present processing procedure therefore does not identify whether the weaker component in the received signal precedes or follows the stronger one.

Some general features of the real cepstrum (figs. 13 and 14) can be explained. Large fluctuations at the first few cepstrum points are the result of the general shape of the DFT, which is large over the range of frequencies where the carrier tones are located, and falls off to either side. After taking the logarithm of the DFT magnitude, there results the general form shown in Fig. 15. Additional distinctive features are a peak corresponding to the channel spacing, (at point #75 in Figs. 13 and 14) and a large ripple centered at the baud rate (point #109 in Fig. 14). The remaining irregular cepstrum waveform is relatively small and contains the detailed signal information.

A common component of the various signal cepstra emerges when a number of distinct signal cepstra are averaged, as shown in Fig. 16. The degree of variability around this common component is illustrated by the max. and min. plots in Fig. 18, which are based on a comparison of nine distinct signal cepstra. Fig. 17 shows a plot of the estimated standard deviation at each cepstrum point, based on the same nine signal cepstra.

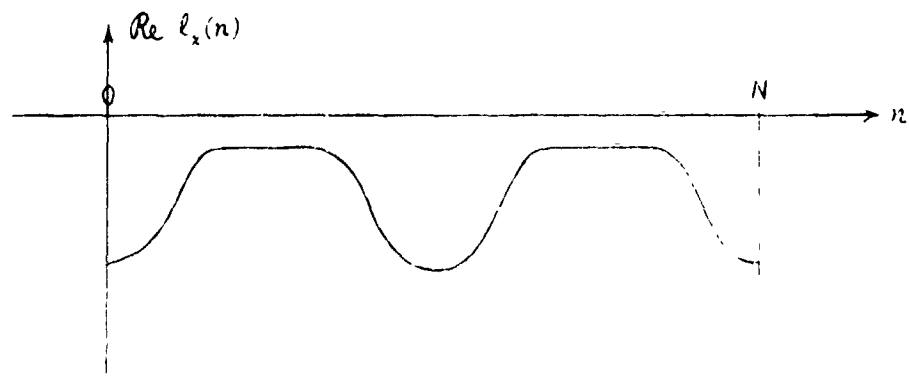


Fig. 15 Sketch of general trend of the discrete logarithmic spectrum

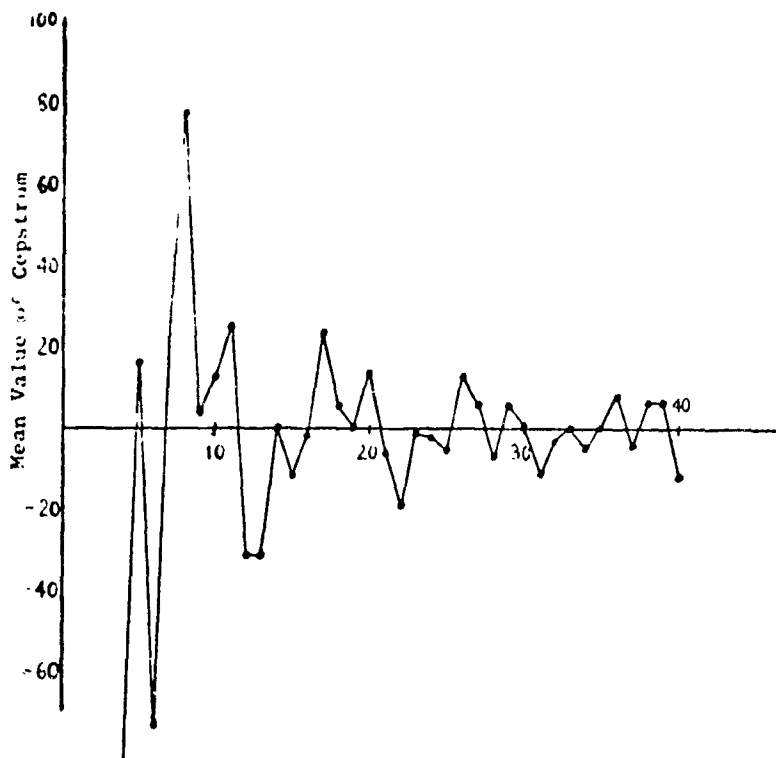


Fig. 16 Mean value of PSK signal cepstrum, when averaged over 9 different signal samples with independent random modulation. (First 40 points)

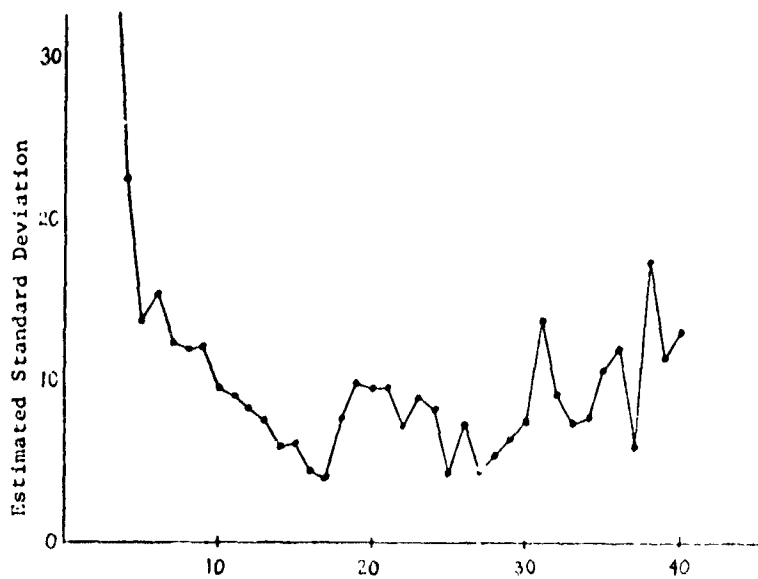


Fig. 17 Estimated standard deviation at the first 40 points for 512-point signal cepstra.

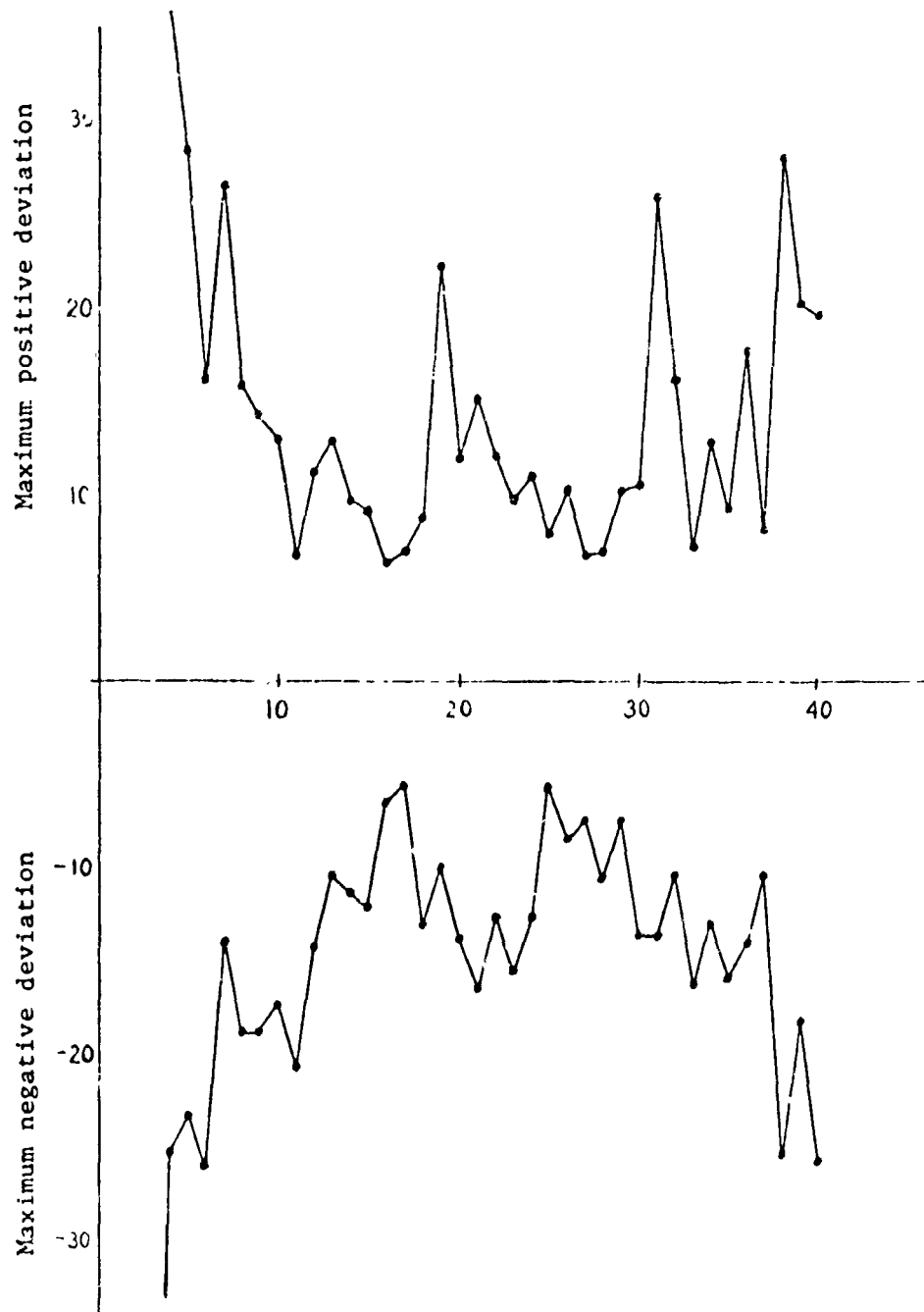


Fig. 18 Maximum positive deviation from mean and maximum negative deviation from mean, for the first 40 points of the signal cepstrum

5. THE COMPUTER PROGRAM

The computer program for multipath processing which has been developed exists in the form of a FORTRAN punched-card deck of approximately 550 cards for operation in the Honeywell (formerly GE) 635/645 computer at RADC. The organization and use of this program is described in this chapter.

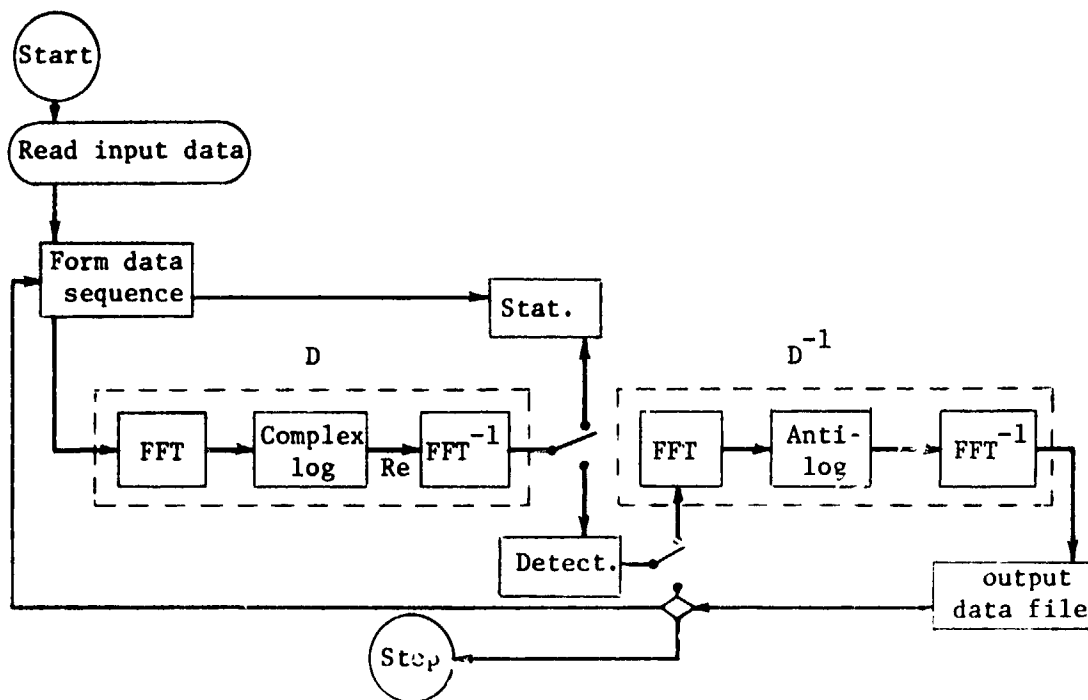


Fig. 19 Overall Functional Block Diagram of Computer Processing System

5.1 General Description

Fig. 19 is a block diagram of the major program functions as described in this Section, exclusive of the various plot and printout features.

The program reads and retains the contents of an input data file. It selects from this data a record of specified length. This record constitutes the signal sample sequence which is processed during one "pass".

The signal data undergoes the transformation D as described in Sec. 2.2, with the exception that only the real part of the complex logarithm is utilized for the generation of the cepstrum. The real part of the cepstrum is plotted, and the values of both the real and imaginary part are printed out. After this, there are two possibilities. If statistical data is to be collected about the properties of the cepstrum (for use in the multipath detection system), then a suitable routine can be entered which records information about the first 100 points of the cepstrum. Thereafter, the next data sequence will be processed. After a specified number of passes, the mean, standard deviation, min. and max. at each of the first 40 cepstrum points, will be computed and printed out.

If, on the other hand, multipath processing is to be carried out, then the program directs control to the multipath detection subroutine. It examines the cepstrum for the possible presence of a multipath structure. If a sufficiently prominent multipath effect is detected so that it can be reasonably clearly identified, the strength and time delay of the multipath component is estimated and this information is printed out. At this point there exists the option of terminating the "pass", and initiating the next pass. Otherwise, the cepstrum of the calculated multipath component is constructed, and printed out, and its FFT computed. The latter is then subtracted from the complex log of the input signal spectrum so that, ideally, the contribution of the multipath is now neutralized. Subsequent exponentiation and inverse F.T. completes the D^{-1} transformation. The reconstructed signal thus obtained is recorded into the output data file. Control may then be returned to the beginning of the program for another "pass", utilizing the next set of data samples in the input data file.

Provisions for optional table print-outs and plots are also incorporated at various stages of processing.

5.2 Data Files

As presently set up, the program works with several BCD data files. These are defined as permanent files emanating from the user's master catalog, as follows:

<u>File name</u>	<u>Function</u>
F1	input data file
C1	output file
M1	mean signal cepstrum
T1	threshold levels
W1	weights used in multipath detection

In order to conserve file space, the files have been written with five entries per record, using the format

(1X, E13.6, 1X, E13.6, 1X, E13.6, 1X, E13.6, 1X, E13.6)

The input data file contains the signal sample to be processed. The program reads the entire input file, into the array XIN, which is presently set up for 1360 sample values. A change in this number can be effected by revising the READ statement for F1 and by changing the dimension of XIN in the COMMON statement in the main program and in subroutines SPLT, SPIOT, GEN, and STAT.

The portion of the input data which is to be processed in any one "pass" is identified on the data card by specifying the index in the array XIN which is the beginning of the sample sequence to be processed.

The contents of files M1 and T1 are determined on the basis of measurements on the type of signal to be processed. (These measurements are performed in the STAT subroutine.) The contents of files M1 and T1 are read by the DET subroutine.

In file W1 are stored a set of weights, or correction factors, which depend on the data window shape (see Sec. 5.3.6). If, during

the detection process, a multipath cepstrum spike is detected at position k , then its magnitude gets multiplied by the weight for that position, in order to yield an improved estimate of the multipath gain α .

5.3 The Main Program and Subroutines

The detailed arrangement of the main program is apparent from the flow chart in Fig. 20. It performs the operations described in Section 5.1. However, all the major computational steps are carried out in the various subroutines. Communication between the main program and subprograms is through COMMON and the subroutine calling sequences.

The major program functions to be executed are selected by assigning the appropriate value to the variable IST. This value is entered as data when running the program. IST has the following effect:

- IST = 0 computation of cepstrum, multipath detection, and reconstruction of input signal with multipath removed.
- IST = 1 computation of cepstrum and gathering of statistics on the first 100 cepstrum points.
- IST = 2 computation of cepstrum and multipath detection.

The program is arranged to provide the following printer outputs:

- 1) A plot of the real part of the cepstrum, and a listing of the real and imaginary parts.
- 2) A listing of the estimated multipath cepstrum.
- 3) A listing of the log-spectrum of the corrected signal.
- 4) A listing of the spectrum of the corrected signal.
- 5) A listing of the corrected signal, under the heading "BASE FUNCTION RESULT".

In addition to these, various choices of output can be selected by assigning the appropriate value to the variable IOUT. These choices pertain to

- 1) the input data
- 2) the input spectrum (if plotted, it is the magnitude spectrum)
- 3) the log spectrum of the input.

The value of IOUT is entered as data when running the program. IOUT has the following effect:

IOUT = 1 print out tables of data only
IOUT = 2 plot graphs only
IOUT = 3 print out tables and plot graphs
IOUT = 4 no output
IOUT = 5 data is stored in file C1

The main program COMMON statement specifies the following dimensioned arrays:

X(2,512,2), XIN(1360), XV(512,2), CP(512), XM(100,9) .

If data records of more than 512 samples are to be processed in one pass, the dimensions of some of the arrays have to be changed in all the COMMON statements where those arrays occur.

5.3.1 Subroutine FFT - Fast Fourier Transform

This subroutine is an adaptation of the FFT program described in [4]. It performs both the forward and inverse FFT, as selected by the value of the variable SGN in the following way:

SGN = -1. forward transform
SGN = +1. inverse transform

The value of SGN is set in the main program, and in the subrouting DET, prior to calling FFT.

The subroutine operates on the data contained in the array X(1,I,J), and the result is again entered in X(1,I,J). The second argument, I, identifies a particular (complex) data sample, and the third argument, J, identifies the real and imaginary parts:

J = 1 real part
J = 2 imaginary part.

The calling sequence for FFT is

(N, NSTAGE, SGN),

where

N is the number of samples in the signal record to be processed (a power of 2)

NSTAGE is the binary logarithm of N

SGN as described above.

The values of N, NSTAGE are read from a data card by the main program.

5.3.2 Subroutine CLOG - Complex Logarithm

This subroutine computes the complex logarithm of the data contained in the array X(1,I,J) and returns the result into the array X(1,I,J). The magnitude of the real part of the logarithm has been delimited in the negative direction so that it does not exceed a value of $6 \ln 10$ below the logarithm of VMAX, where VMAX is computed in the main program as the maximum absolute value appearing in the array X(1,I,J). The imaginary part of the logarithm is computed in accordance with the algorithm described in [5].

The subroutine also assigns values to the variables XB, X1, and K1 as follows:

XB argument of sample number $N/2 + 1$ (within CLOG, this variable is called XM).

X1 argument of sample number 1 (the zero-frequency sample) after XB has been subtracted.

K1 magnitude of linear phase component that has been subtracted (see [5].)

The calling sequence for CLOG is

(N, DIV, XM, XL, K1),

where

DIV is VMAX times 10^{-6} (assigned in main program) and all other variables have been described.

5.3.3 Subroutine CALOG - Antilogarithm

This subroutine computes the antilogarithm of the contents of the array X(1,I,J) and returns the result into X(1,I,J). It also

assigns the polarity of the zero-frequency sample in accordance with the value that was assigned to the variable X1 in CLOG.

The calling sequence for CALOG is
(N,X1).

5.3.4 Subroutine SPLT - Plot Routine Driver

This subroutine performs various chores in connection with the plotting operation, and calls the plotting subroutine SPLOT.

When a plot is called for by the main program, it transfers the data to be plotted into the array XV(512,2) prior to calling SPLT. If the plot is to display absolute magnitudes of complex numbers, then SPLT replaces the real parts contained in XV(I,1) by the absolute values. Then it prints the header "REAL" (if a magnitude plot or a plot of the real components is to follow) or "IMAG" (if a plot of imaginary components is to follow). If a cepstrum plot is to be made, it sets the first and last four samples of the cepstrum data equal to zero. (This is to avoid an excessive compression of the ordinate scale of the plot, which otherwise results from the very large values of the cepstrum near the endpoints.)

The maximum and minimum values of the data to be plotted are then determined and assigned to variable, YMAX and YMIN, respectively. In case YMAX = YMIN, no plot results. The number of points to be plotted is then selected and assigned to NN, and the subroutine SPLOT is called to carry out the actual plotting operation.

The calling sequence for SPLT is
(ISUB, INN, IP, NN),

where

ISUB, INN and IP are set in the main program and specify what type of data is to be plotted

NN this variable carries the value of the variable N in the main program.

5.3.5 Subroutine SPLOT - Plot

This subroutine is set up to plot data on either the high-speed line printer or on the teletype terminal. The difference between the two is the line size, which is set when calling this subroutine by assigning either the value 101 (line printer) or 61 (teletype) to the variable LSZ.

The subroutine selects an ordinate scale such that the values of YMAX and YMIN fall within the range of the scale. The scale is selected in such a way that major subdivisions occur either at multiples of 10, of 5, or of 2. The data is then plotted to the scale which has been selected.

The calling sequence for SPLOT is

(YMIN, YMAX, NN, LSZ)

where NN determines the number of points to be plotted, and is assigned in SPLT; and the other variables are also assigned in SPLOT, and have been described.

5.3.6 Subroutine GEN - Data generator

The purpose of this subroutine is to generate a data sequence of specified length N for processing, from the input data XIN, beginning at position IFL of the input data. It also applies a "Hanning" window to the data, by weighting the first and last 25 data points by a raised cosine curve.

The calling sequence for GEN is

(N, IFL)

where both N and IFL are read from a data card at the beginning of a pass.

5.3.7 Subroutine STAT - Statistics Collector

This subroutine collects various statistics over several passes through successive data sequences, during one run of the main program.

For each of the first 100 cepstrum points, it determines

- a) the average value
- b) the standard deviation
- c) the maximum excursion above the average
- d) the maximum excursion below the average

over several passes. Data enters this subroutine in the array XM(100,9). The results are printed out in a table.

The calling sequence for STAT is

(ITMQ),

where ITMQ is read from a data card by the main program and determines the number of passes which are to be processed. The program is presently dimensioned to handle a maximum of 9 passes during one run.

5.3.8 Subroutine DET - Multipath Detection

In this subroutine the real cepstrum of the input signal sample sequence is examined for the possible presence of a multipath component. If the presence of a multipath component is determined, the magnitude and delay of the multipath characteristic are estimated in the manner described in Sec. 6.1 and 6.3. The detection procedure is presently set up to operate on the set of cepstrum samples beginning with number 2 and ending with number 40. (The upper limit is set by the variable IRNG.) The arrangement of the subprogram is described graphically in the simplified flow chart in Fig. 21.

This subprogram produces the following printed output:

- a) If no multipath component is detected in the specified range of the cepstrum, then the output is "NO MULTIPATH DETECTED". Also printed are:
 - 1) the index of the cepstrum sample (the variable M) which deviated most from the recorded mean value;
 - 2) the value C(M), which is the cepstrum at M; and
 - 3) the amount by which this value differs from the recorded mean at M.

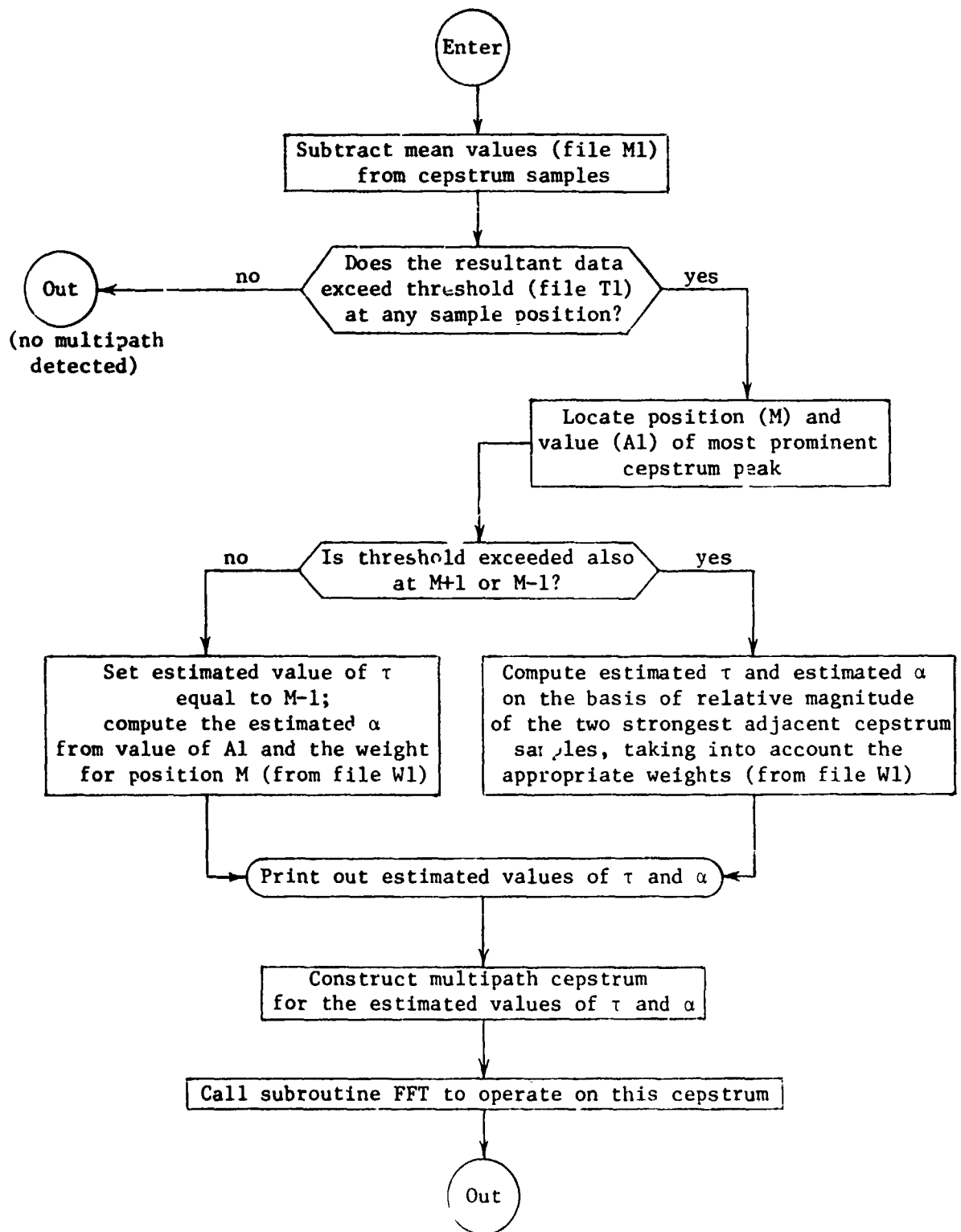


Fig. 21 Simplified flow chart for subroutine DET.

- b) If the multipath is found to be present with a delay that is essentially an integer multiple of a sampling interval, the output is "MULTIPATH DETECTED AT C(M)". Also printed are:
- 1) the index of the cepstrum sample (the variable M) at which the largest multipath spike occurs
 - 2) same as item (2) above; and
 - 3) same as item (3) above
 - 4) the preset detection threshold at M;
 - 5) the estimated multipath delay τ (the variable TU)
 - 6) the estimated multipath gain (the variable A1)
 - 7) the synthesized multipath cepstrum
- c) If multipath is found to be present with a delay that is not estimated to be an integer multiple of a sampling interval, the output is "MULTIPATH DETECTED BETWEEN C(M) AND C(M+1)". Either the + or the - sign appears. M always designates the index at which the greatest deviation of the cepstrum from the mean value occurs. If the next sample exceeds the preset threshold, the + sign applies. If, instead, the preceding sample also exceeds the preset threshold, the - sign applies.

Also printed are:

- 1) The value of M
- 2) The same information listed under (2), (3), (4) of (b), for both M and M+1
- 3) The estimated multipath gain if only the cepstrum at M is considered (the variable A1)
- 4) The estimated multipath gain based on C(M) and C(M+1) (the variable A2)
- 5) The estimated multipath delay τ (the variable TU)
- 6) The synthesized multipath cepstrum.

The calling sequence for DET is

(NN, NSTGE)

where NN is the variable which carries the value of the variable N in the main program, and NSTGE has been described

5.4 Running the Program

In order to operate the program, the signal data to be processed must first be loaded into file F1, using the format described in Sec. 5.2. If the detection parameters which are stored in files M1, and T1 are applicable to the signal to be processed, then the program can be run in the detection mode. This requires only preparation of the appropriate data cards and appending them to the program.

The first data card bears only a single integer, format (3X,I2). This is the value to be assigned to ITMQ, which is the number of passes to be made in a single execution of the program.

As many data cards as the specified number of passes must then follow, one data card for each pass. Each of these data cards bears the values to be assigned to N, NSTGE, IOUT, IFL, and IST, using the format (3X,I4,3X,I2,3X,I1,3X,I4,1X,I1). The significance of N and NSTAGE are explained in Sec. 5.3.1, IOUT and IST in 5.3, IFL in 5.3.6.

If the detection parameters which are stored in files M1 and T1 are not applicable to the signal to be processed, statistics on the signal cepstrum (without multipath) must first be computed. The procedure for this is the same as described above. The mean values for the cepstrum which are computed in the STAT subroutine must be loaded into file M1. Also, on the basis of standard deviations and peak deviations from the mean, as obtained in the STAT subroutine, detection thresholds must be established and loaded into file T1.

6. SYSTEM PERFORMANCE

6.1 Detectability of the Multipath Cepstrum

In the present implementation, as described in the previous Chapter, detection of the multipath cepstrum (that is, determination of the presence of multipath) consists of simple threshold detection of the strongest cepstrum value over that portion of the cepstrum that is of interest. This permits reliable detection of multipath over a significant range of α and τ . The following discussion is based on results that have been obtained with the synthesized 16-channel PSK signal as described in Section 4.1, sampled at 8175 samples/sec., and processed in 512-point sequences. With this sampling rate, a multipath delay of less than 4 ms will result in the strongest multipath cepstrum spike to occur somewhere within the first 34 cepstrum samples.

The detection characteristic depends on the threshold setting. In Sec. 4.3, the variability of the signal cepstrum was described in terms of measured standard deviations, means, and peak deviations from the mean. The threshold setting then determines the probability of false alarm (detection of multipath when none is present). Only a crude estimate of false-alarm probability is possible, for a given threshold setting, on the basis of these assumptions:

- a) Successive samples of the signal cepstrum are characterized by independent random variables.
- b) These independent random variables are approximately Gaussian.
- c) Additional variability due to signal truncation and the effect of the window function is negligible. (This essentially says that such additional variability is already accounted for in the model as assumed under (a) and (b).)

Proceeding on the basis of these assumptions, suppose that the threshold is set at

$$\theta_n = \mu_n \pm 3\sigma_n, \quad (6-1)$$

where θ_n is the threshold at the nth threshold sample,

μ_n is the estimated signal cepstrum mean value at the nth cepstrum sample,

σ_n is the estimated standard deviation of the signal cepstrum at the nth cepstrum sample.

Let X_n denote independent Gaussian random variables with mean μ_n and standard deviations σ_n , with $n = d_1, \dots, d_2$, where d_1, d_2 are the limits of the detection range. If the detection range extends over 32 cepstrum points, then the probability of false alarm becomes

$$\begin{aligned} p_f &= 1 - [P(|X_n - \mu_n| < 3\sigma_n)]^{32} \\ &= 1 - .9973^{32} \approx 0.08. \end{aligned}$$

This is actually a pessimistic estimate, since (a) some correlation between cepstrum samples surely exists, and (b) available data indicates that peak variations in the signal cepstrum tend to be fairly restricted. Of course, in order to improve the detectability of weak multipath, the threshold has to be lowered, which also increases the probability of false alarm.

For arbitrary threshold settings θ_n , the probability of missing a multipath spike at position n (assuming τ to be a multiple of the time between samples) with magnitude $\alpha = \theta_n$ is

$$p_m = 1/2.$$

However, as discussed in Sec. 3.3, if τ is not an exact multiple of the sampling interval, then the largest multipath cepstrum component is reduced in magnitude, for the same α . This reduction is given by $\text{sinc } v$, where v denotes the difference between τ and the nearest integer multiple of the time between samples. The mean height of the largest multipath cepstrum component, averaged over τ , is therefore

$$\int_{-1/2}^{1/2} \text{sinc } v \, dv = \frac{2}{\pi} \text{Si}(\pi/2) = 0.87.$$

Again using the Gaussian assumption, the probability of missing a multipath component with $\alpha = \theta_n$ is therefore greater than 1/2. If the thresholds are set according to (6-1), then the multipath cepstrum corresponding to $\alpha = 3\sigma$ reaches on the average only $.87 \times 3\sigma_n = 2.61\sigma_n$, or $.39\sigma_n$ below threshold, so that the detection probability in the case $\alpha = 3\sigma_n$ is actually only about 0.35.

It is to be noted that a "false alarm" and a "miss" can occur simultaneously. While a weak multipath spike may be present that does not reach threshold, the signal cepstrum might exceed threshold at a different point.

A reasonable threshold function, based on the signal data in Chapter 4, results in a detection region about as shown in Fig. 22, where the threshold curve has been smoothed, for easier viewing. Also entered in this Figure are several contours of detection probability, which have been estimated on the basis of the above assumptions. The rise of these contours for large τ is due to the degradation in the multipath cepstrum as a result of truncation of the input signal (see Sec. 3.4).

There is another effect which does not appear in Fig. 22. Because the threshold increases sharply for very small τ , it is possible that the first cepstrum spike of a multipath characteristic having moderate α and small τ goes undetected, whereas the second spike is detected since it falls into a lower threshold region. Of course, no useful multipath correction can be accomplished in that case, so that it can be classified as the simultaneous occurrence of a "miss" and a "false alarm".

6.2 Effect of Error in Estimating the Magnitude of the Multipath Component

The cepstrum of a single multipath component with delay τ (τ assumed a multiple of the sampling interval, $\tau = \frac{rT}{N}$ and relative gain

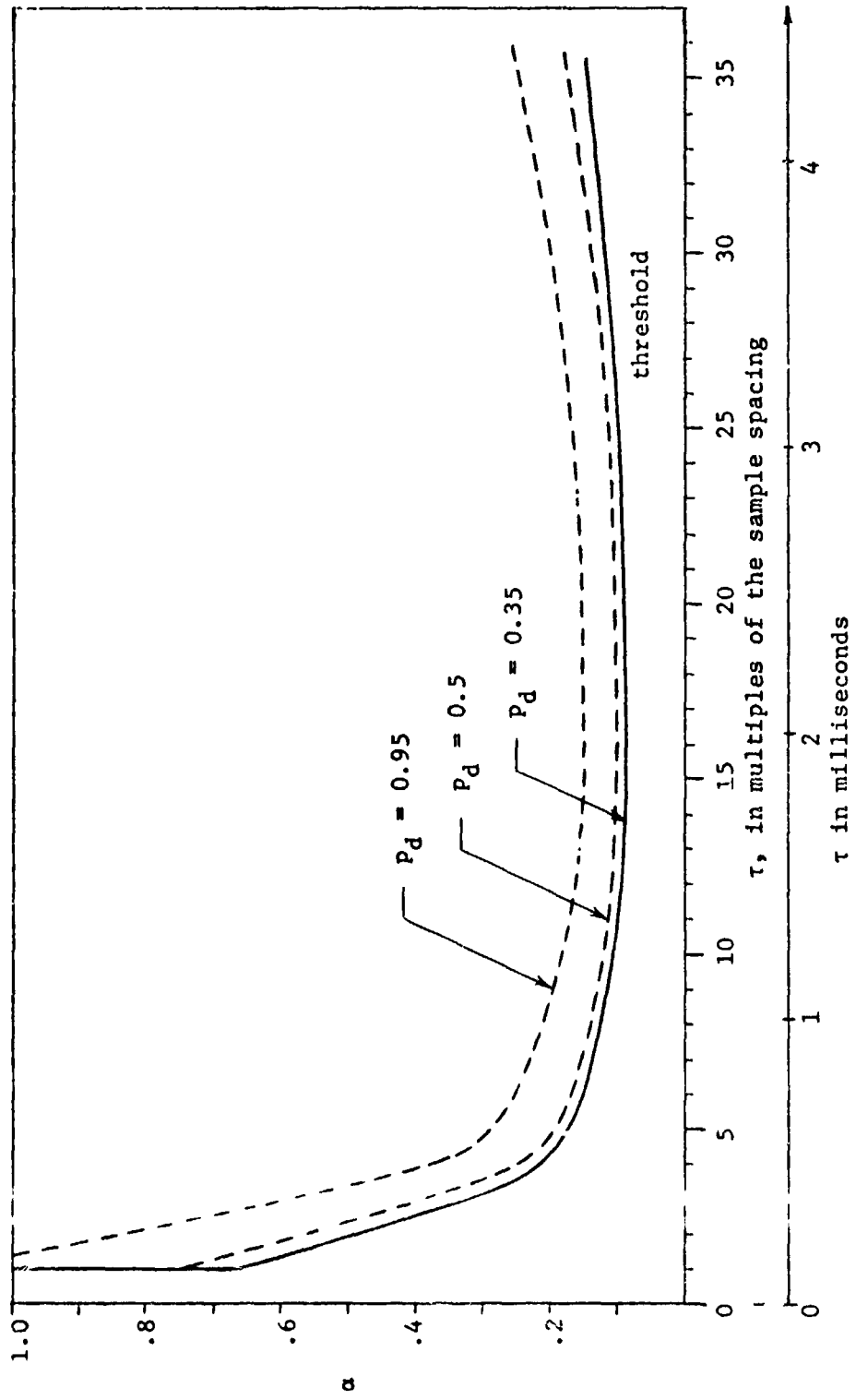


Fig. 22 Multipath Detection Characteristics.

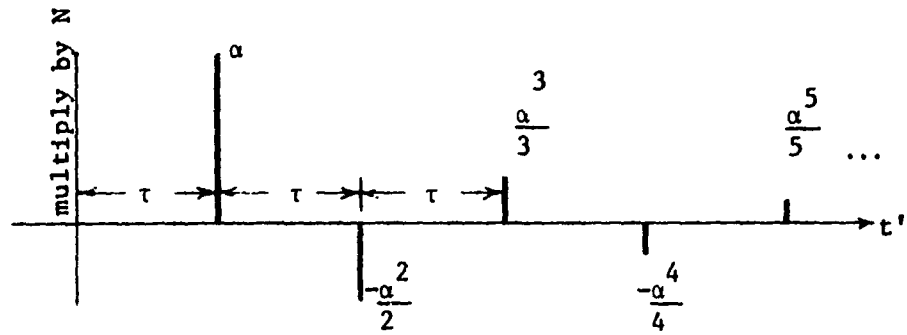
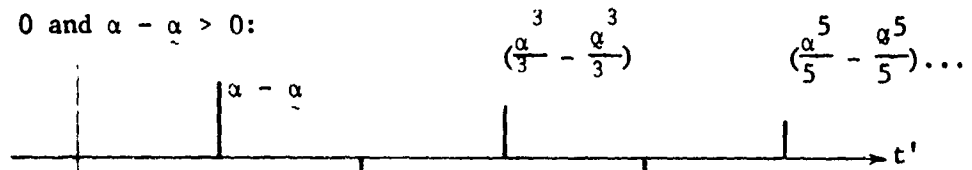
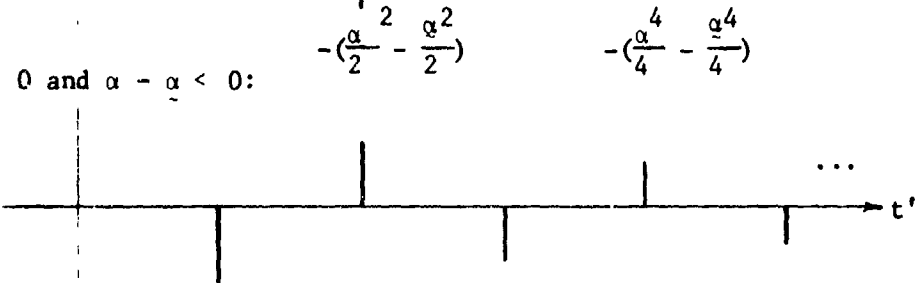


Fig. 23 Multipath cepstrum

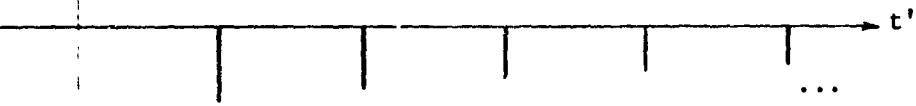
a) $\alpha > 0$ and $\alpha - \alpha > 0$:



b) $\alpha > 0$ and $\alpha - \alpha < 0$:



c) $\alpha < 0$ and $\alpha - \alpha < 0$:



d) $\alpha < 0$ and $\alpha - \alpha > 0$:

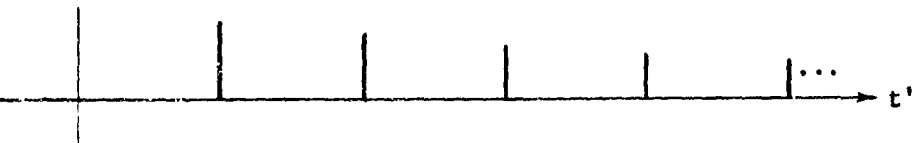


Fig. 24 Residual Cepstrum Pattern after imperfect cancellation.

α is as shown in Fig. 23. If the estimated multipath gain is $\underline{\alpha} \neq \alpha$ then subtraction of the synthesized multipath cepstrum based on gain $\underline{\alpha}$ from the actual multipath cepstrum leaves a residual cepstrum pattern which appears in one of four ways shown in Fig. 24

None of these patterns represent a single residual multipath component, but a sequence of multipath contributions with delays $\tau, 2\tau, 3\tau, \dots$. The same analysis applies to all four cases, and is conveniently carried out in terms of z-transforms. Let

$c_{\alpha,r}$ denote the actual multipath cepstrum at delay r samples, magnitude α ;

$c_{\underline{\alpha},r}$ denote the estimated multipath cepstrum at delay r samples, magnitude $\underline{\alpha}$.

Subtraction of $c_{\underline{\alpha},r}$ gives the residual cepstrum $c_{\alpha,r} - c_{\underline{\alpha},r}$. Applying the DFT gives, in the discrete complex logarithm domain:

$$\text{cIn} (1 + \alpha z^{-r}) - \text{cIn} (1 + \underline{\alpha} z^{-r}) = \text{cIn} \frac{1 + \alpha z^{-r}}{1 + \underline{\alpha} z^{-r}} \quad (6-2)$$

Exponentiation gives

$$\frac{1 + \alpha z^{-r}}{1 + \underline{\alpha} z^{-r}} = 1 + (\alpha - \underline{\alpha})z^{-r} - \underline{\alpha}(\alpha - \underline{\alpha})z^{-2r} + \underline{\alpha}^2(\alpha - \underline{\alpha})z^{-3r} - \dots \quad (6-3)$$

This series is the z-transform of a transfer function consisting of a sequence of impulses, corresponding to multiple paths, or a tapped delay line (Fig. 25).

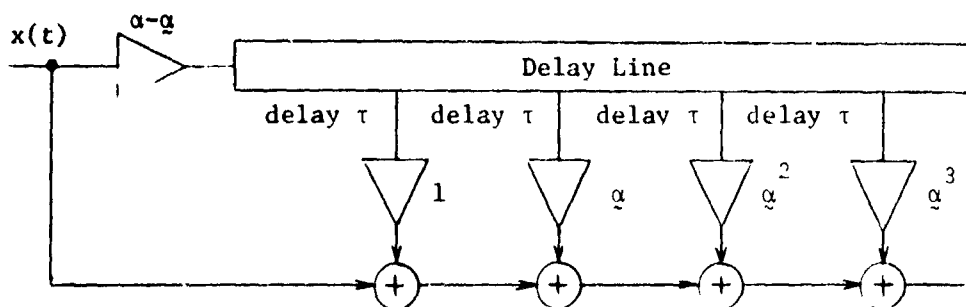


Fig. 25 Tapped delay line representation of residual error

As rough measure of performance, a signal-to-interference ratio can be computed under the assumption that the superimposed delay components are uncorrelated. First, at the receiver input, a single multipath component with relative strength α gives an r.m.s. signal-to-interference ratio

$$R_i = V_s/V_m = V_s/|\alpha|V_s = \frac{1}{|\alpha|}, \quad (6-4)$$

where

V_s = r.m.s. signal voltage

V_m = r.m.s. multipath interference voltage.

After the cepstrum processing described above, there results a superposition of many residual multipath components, resulting in a m.s. value of

$$V_s^2(\alpha - \alpha)^2 [1 + \alpha^2 + \alpha^4 + \dots] = V_s^2 \frac{(\alpha - \alpha)^2}{1 - \alpha^2}. \quad (6-5)$$

The r.m.s. output signal-to-interference ratio is therefore

$$R_o = \frac{\sqrt{1 - \alpha^2}}{|\alpha - \alpha|} \quad (6-6)$$

The improvement in signal-to-interference ratio as a result of cepstrum processing is then

$$\frac{R_o}{R_i} = \frac{\sqrt{1 - \alpha^2}}{|1 - \alpha/\alpha|}. \quad (6-7)$$

In Figure 26, contours of this function are plotted vs. α and α . In the region where $\frac{R_o}{R_i} < 1$, an actual degradation results.

However, the output signal-to-interference ratio alone may be of interest. Thus, it may be asked, to what portion of Fig. 26 must operation be confined in order that the signal-to-interference ratio after processing does not exceed a specified value. This question is answered in Figure 27. There, contours of $R_o = 10$ (20 db signal-to-interference ratio) and $R_o = 5$ (14 db ratio) are plotted.

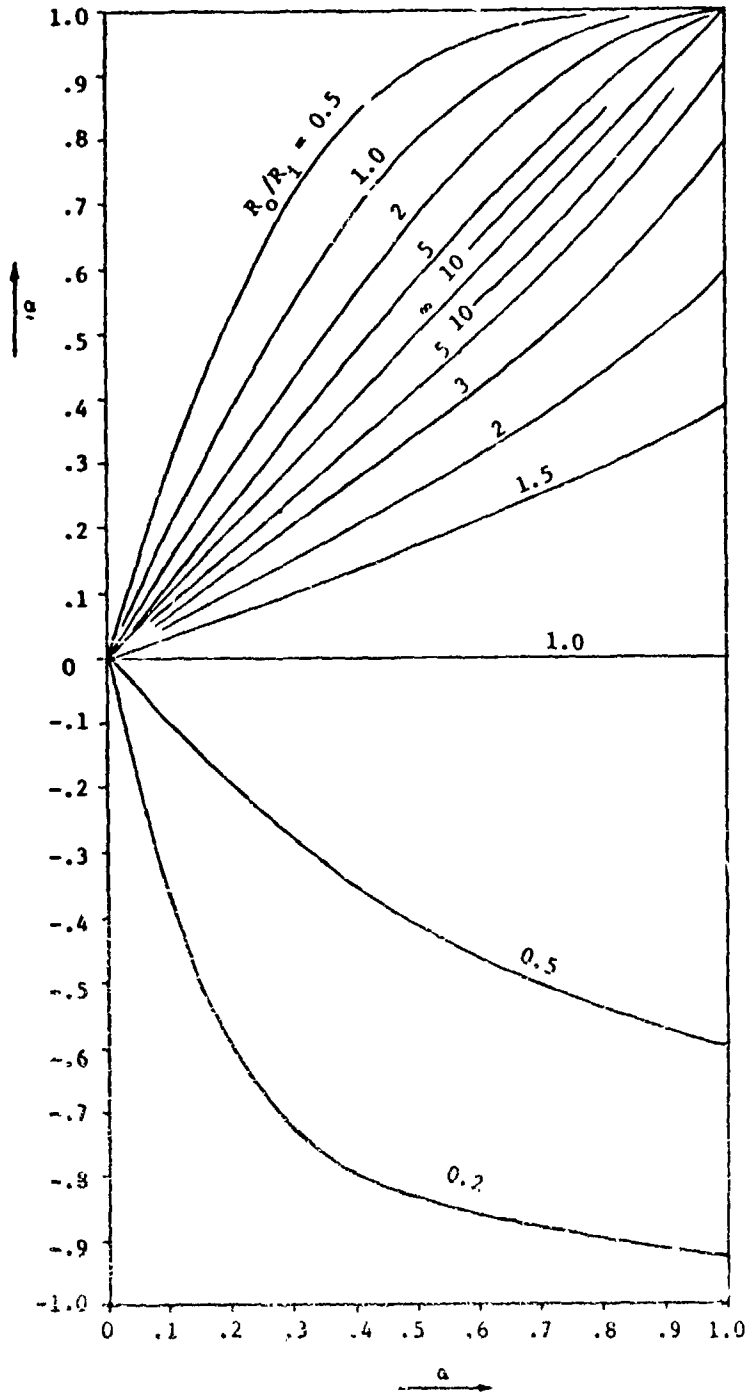


Fig. 26 Improvement in Signal-to-Interference Ratio

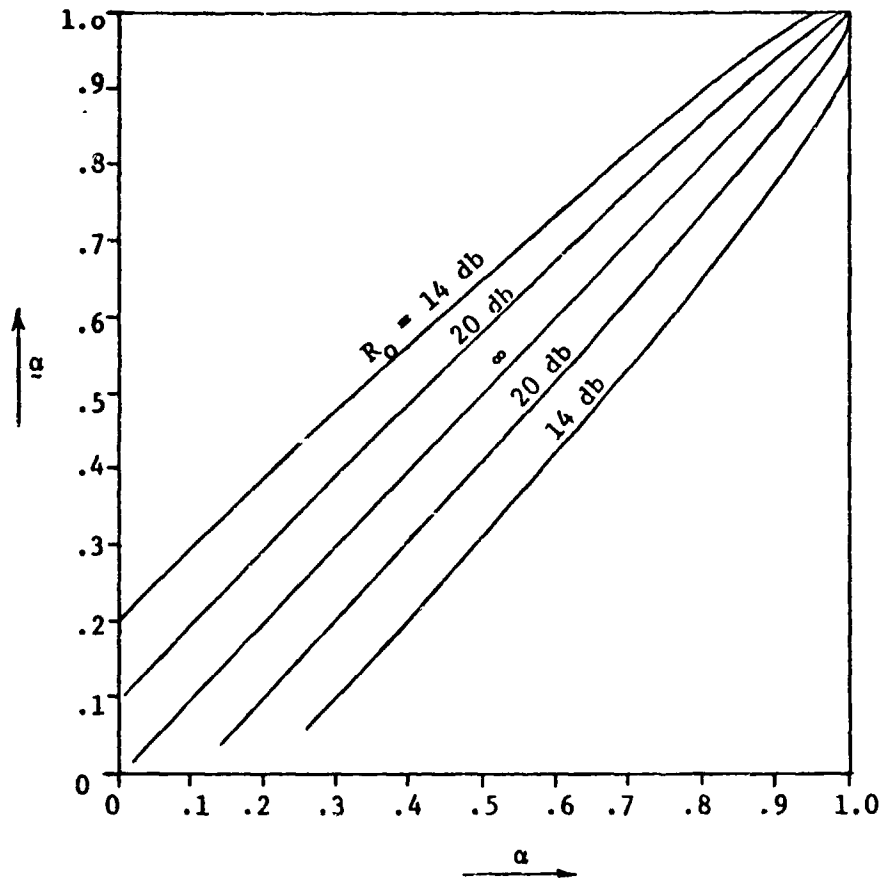


Fig. 27 Output Signal-to-Interference Ratio Related to Error in the Estimated Multipath Amplitude

The effect of compensating for only one multipath component, when actually several multipath components exist, can be analyzed in a similar manner. Suppose the received signal is of the form (2-9). For simplicity, assume $\tau_i = \frac{r_i T}{N}$, $i = 1, 2$. Without considering the multipath cepstrum, it is easily seen that in this case (6-2) becomes

$$\text{c} \ln(1 + \alpha z^{-r_1} + \beta z^{-r_2}) - \text{c} \ln(1 + \alpha z^{-r_1}) = \text{c} \ln \frac{1 + \alpha z^{-r_1} + \beta z^{-r_2}}{1 + \alpha z^{-r_1}} \quad (6-8)$$

Exponentiation gives

$$\frac{1 + \alpha z^{-r_1} + \beta z^{-r_2}}{1 + \alpha z^{-r_1}} = \frac{1 + \alpha z^{-r_1}}{1 + \alpha z^{-r_1}} + \frac{\beta z^{-r_2}}{1 + \alpha z^{-r_1}} \quad (6-9)$$

The first term on the right is the same as (6-3). The additional term expands to

$$\beta z^{-r_2} - \beta \alpha z^{-(r_1+r_2)} + \alpha^2 \beta z^{-(2r_1+r_2)} - \dots \quad (6-10)$$

This shows that besides leaving the second multipath component untouched (the term βz^{-r_2}), an additional sequence of delay components is introduced at delays of r_1+r_2 , $2r_1+r_2$, etc.

6.3 Extraction of Multipath Information

Assuming that a multipath component has been detected, the error in extraction of the multipath information can then be discussed.

It has already been mentioned that the present system does not yield polarity of τ . This point is considered further in Sec. 7.1.

Based on Equ. (3-22), the present method of estimating τ consists of fitting a sinc-function to two adjacent cepstrum samples, if both these samples exceed the threshold. The center of the sinc-function then gives the estimated value of τ . If the two cepstrum samples which straddle the true value τ both fail to reach threshold, no multipath is detected. If only one of them exceeds threshold, then the estimated multipath delay is taken as the position of that sample.

The error in $\hat{\tau}$, the estimated multipath delay (aside from polarity) can therefore be assumed to be restricted to within one sampling interval of the true value, giving $|\hat{\tau} - \tau| < .122$ ms, and the accuracy improves with increasing α . A precise statement is not easy to formulate because the accuracy of the estimate $\hat{\tau}$ depends also on the relation between τ and the sampling intervals. If τ is an exact multiple of the sample spacing, then by definition of "detection" of the multipath cepstrum spike, $\hat{\tau} = \tau$.

Extraction of the multipath gain α can be characterized graphically in the manner shown in Fig. 28, which applies for a range of τ for which the threshold is set for approx. 0.1 (see Fig. 22). The probability contours in Fig. 28 are based again on the data of Ch. 4, and the simplifying assumption that the signal cepstrum values are governed by Gaussian r.v.'s.

Comparison of Fig. 28 with Figs. 26 and 27 yields the probability with which a specified reduction in interference or a specified output signal-to-interference ratio can be achieved.

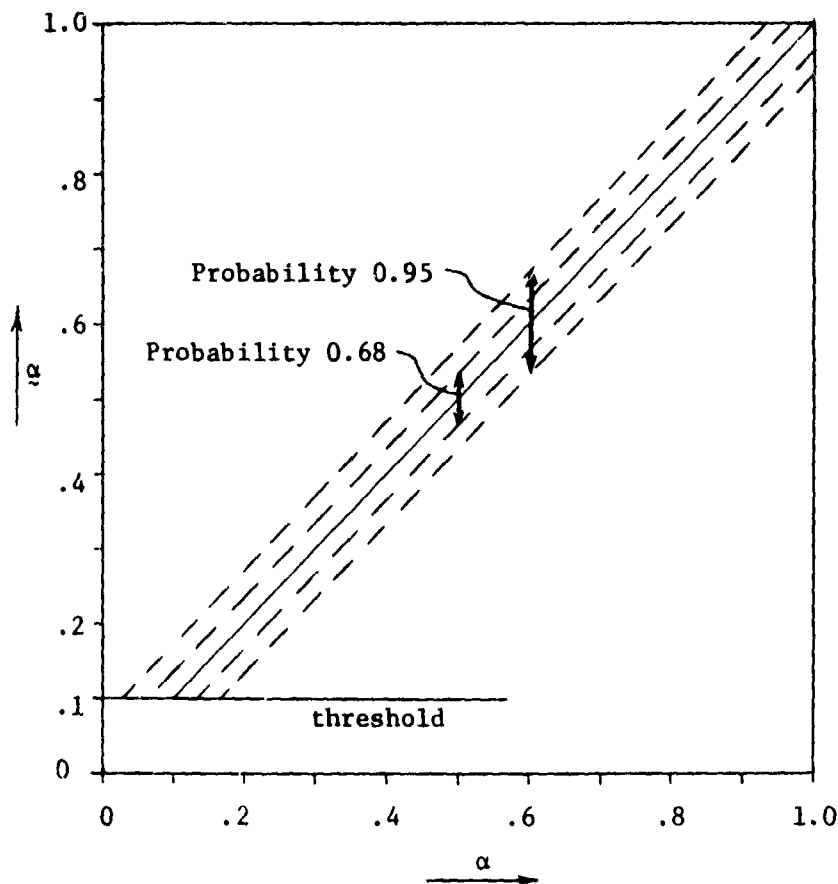


Fig. 28 Extraction of the Multipath Magnitude, for $\tau \approx 2$ ms.

6.4 Reconstruction of Transmitted Signal Component

In the absence of multipath, straight-through processing of the input signal via the D and D^{-1} blocks of Fig. 19 leads to an output which contains negligible error. This has served as a check on the sub-routines FFT, CLOG, and CALOG, and demonstrates that there is no significant build-up of round-off errors. However, when using the program in the multipath detection mode, the reconstructed signal appearing at the output cannot be expected to be "pure", due to errors in the estimates of the multipath parameters (see Sec. 6.2). But even if the estimate were perfect, serious distortions will arise near both ends of the output record due to (a) the end effect described in Sec. 3.6 (see Fig. 11) (b) the data window (see Sec. 3.7).

Therefore, when utilizing the reconstructed signal delivered by the computer program of Ch. 5, it is important that allowance is made for these end effects. The portion of the output record which coincides with the data window, as well as an additional guard space approximately equal to the largest τ to be expected, had best be discarded. This amounts to about 50 points at each end of a 512-point output sequence.

A correction could be applied at the output to reduce the distortion due to the data window. This had not been tried because the other effect (a) would still remain.

7. DISCUSSION

7.1 Possible Improvements in the Present System

The data presented in Chapter 6 shows that with the present system, operating on a synthesized signal, a significant reduction in multipath interference can be achieved with good reliability, and over a wide range of multipath magnitude and delay. This statement assumes that only a single multipath component exists, and that the sign of τ is known. The first of these two restrictions can be overcome by a more sophisticated detection routine which can be implemented as a straightforward extension of the existing detection system. However, the same type of random error in the estimated multipath amplitude, which was described in Chapter 6, appears then independently on each detected multipath component, so that the probability of achieving a specified reduction in the multipath interference is found to be less with several multipath terms than with only a single multipath component (Figs. 26 to 28).

Minor improvements can be achieved by optimizing various system parameters, such as sampling rate, length of data sequence processed in one pass, shape of the data window. Also, various improvements in the detection procedure are possible. For instance, the two largest cepstrum spikes (instead of only the largest one) could be processed in order to achieve an improved estimate of the multipath amplitude and delay. However, such additional refinements (except means of detecting the polarity of τ) will probably contribute little to clarifying the feasibility of the general approach to practical multipath signal processing.

Computation of the phase spectrum from $\{d_x(n)\}$, using the algorithm described in [5], does not yield a unique result. It has therefore not been possible to obtain a meaningful average contribution of the signal cepstrum, which might then be subtracted from each particular realization of the phase spectrum in order to improve detectability of the multipath contribution.

A different arrangement for computing the phase spectrum is proposed which yields a unique result. This can be understood by considering the derivative of $\ln \mathcal{F}_x(f) = \ln |\mathcal{F}_x(f)| + j\psi_x(f)$, where $\psi_x(f)$ is the phase spectrum.

$$\frac{d}{df} \ln \mathcal{F}_x(f) = \frac{\mathcal{F}'_x(f)}{\mathcal{F}_x(f)} = \frac{|\mathcal{F}_x(f)|'}{|\mathcal{F}_x(f)|} + j\psi'_x(f) \quad (7-1)$$

Taking the imaginary part gives

$$\psi'_x(f) = \text{Im} \frac{\mathcal{F}'_x(f)}{\mathcal{F}_x(f)} \quad (7-2)$$

where $\mathcal{F}'_x(f)$ is the F.T. of $(-j2\pi t x(t))$. Application of the inverse F.T. to (7-2) gives (in the t' or cepstrum domain)

$$\mathcal{F}^{-1}_{\psi'_x}(t') = -j2\pi t' \mathcal{F}^{-1}_{\psi_x}(t') \quad (7-3)$$

On the right side of (7-3) appears $\mathcal{F}^{-1}_{\psi_x}(t')$, which is simply the odd part of $\mathcal{C}_x(t')$. This shows that the even and odd parts of the complex cepstrum can be computed separately. The even part is due to the real logarithm of the signal spectrum and can be computed in the standard manner. The odd part of the complex cepstrum is the contribution of the imaginary part of the complex log of the signal spectrum. According to the above, it can be obtained by taking the F.T. of $-j2\pi t x(t)$, dividing by $\mathcal{F}_x(f)$, taking the inverse transform of the imaginary part, and dividing by $-j2\pi t'$.

At first it might appear as if a computational scheme based on the above derivation introduces excessive processing complexity because two different functions have to undergo Fourier transformation, and then inverse transformation. This is not so, however. Because the two functions to be transformed are real and imaginary, respectively, they can be processed simultaneously by the FFT algorithm and their respective contributions separated at the output. Fig. 29 shows how the complete D block (Fig. 19) might be arranged to accomplish this.

Of course, it is not clear whether this method of treating the phase spectrum will be of utility with the PSK signal of Chapter 4.

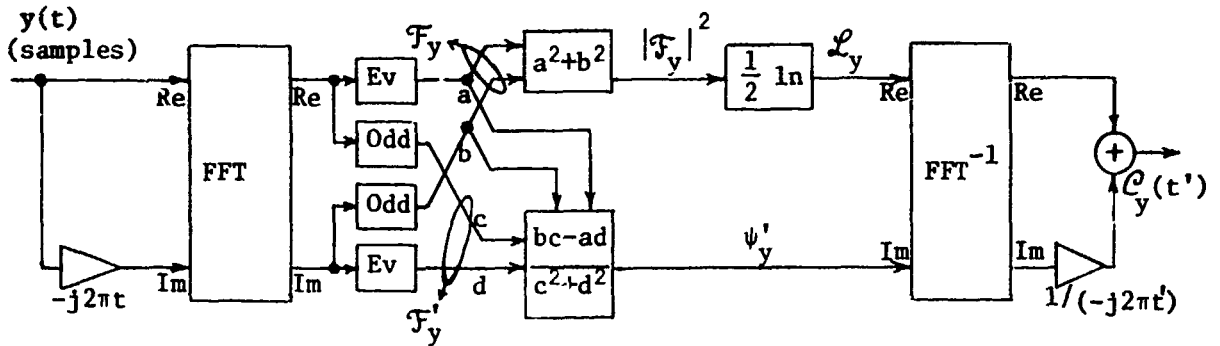


Fig. 29 Alternate Scheme for computing the complex cepstrum

It will have to be determined whether it will result in sufficiently small variability in the odd part of the cepstrum so that useful multipath information can be extracted.

When the communication signals are such that reliable extraction of the polarity of τ is not possible, it is possible to implement a multipath compensator in the following way. Two outputs are provided, corresponding to $+|\tau|$ and $-|\tau|$. The incorrect output can then be rejected either on the basis of human inspection (garbled messages), or automatically on the basis of the quality of a received test waveform.

7.2 Additional Measurements

Tests involving recorded signals from an actual HF modem, direct and as received over an HF link, should turn out to be informative. The full scope of such a test would involve sampling the received signal and recording the binary data on tape. Portions of the tape record then have to be converted into BCD format and stored in the input file described in Sec. 5.2. This data can then be processed and the output stored in the output file. From there, conversion back to binary form and reassembly into a continuous tape record is possible. The reconstructed signal can then be converted back into analog form for demodulation in an actual HF modem.

Such a test would incorporate the influences of many effects which have so far been neglected, such as:

- Sampling jitter, and distortions due to finite duration sampling;
- the exact shape of the PSK waveform as generated in data modems;
- the actual demodulation performance of a data modem;
- the effects of background noise (atmospheric, thermal, and quantization noise);
- possible frequency selectivity of the multipath;
- time variability of the multipath.

A simpler test configuration, and probably more realistic in terms of ultimate implementation, would use the computer to operate on the same data as described above, but only for the purpose of extracting the multipath information. The multipath data can then be collected in a file, and can later be used to control the parameters of a digital multipath filter for cancelling multipath in the test data. For cancellation of a single multipath component, such a filter would be of the form shown in Fig. 30 (cf. [6], and other references cited there). A disadvantage with this digital multipath cancellation filter, however, is the fact that cancellation can occur only at delays which are exact multiples of the time between samples. In other words, a degradation arises due to the quantization of τ . This degradation can be reduced by using a higher sampling rate for multipath cancellation than for multipath estimation.

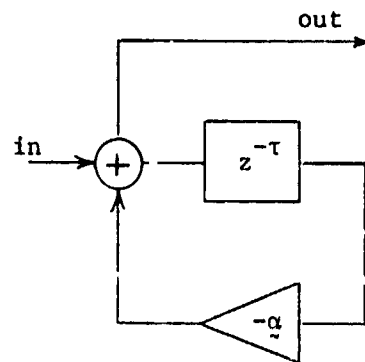


Fig. 30 Recursive Filter for Multipath Cancellation

7.3 Possible Simplifications of the Computer Program

The computer program described in Sec. 5 was developed primarily as a research tool, and is not arranged in the simplest possible manner. The various provisions for output printouts and plots add considerably to the

compile and execution time, as well as memory requirement, and can be deleted in production-type runs. But there are also simplifications possible in the various signal processing steps.

One simplification would result in the elimination of one FFT. In the present system, the FFT subroutine is called four times when multipath cancellation is performed (see Fig. 19). Instead of generating the cepstrum of the estimated multipath and then using FFT, it is possible to generate the exponential of the FFT of the multipath cepstrum directly (see Fig. 31a). This means division, instead of subtraction, to achieve multipath cancellation, but eliminates the need for the CALOG subroutine altogether, as well as one use of FFT. Furthermore, the input signal is now stored and brought forward to the cancellation point in the spectrum domain, instead of the log spectrum domain. Since the imaginary part of the logarithm is not used in multipath detection at present, this means that the complex logarithm routine can be simplified to carry out only the log-magnitude operation.

Further simplification is possible if the program is to be used only to generate multipath data. This results in the block diagram of Fig. 31 b.

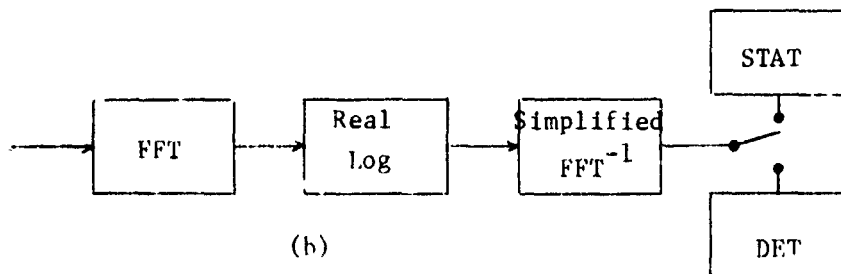
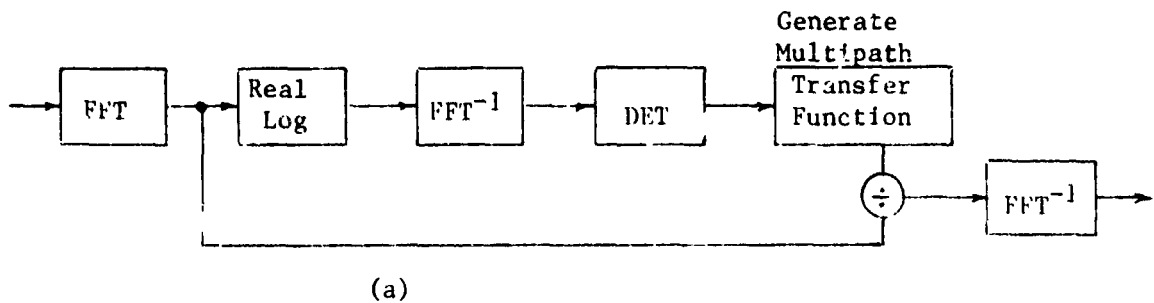


Fig. 31 Simplified Versions of Computer Processor

In this Figure appears a block marked "simplified FFT⁻¹". This is meant to suggest the possibility of a modified version of the FFT for computing only the first 40 (or so) points of the cepstrum, which is the only part of the cepstrum being used for multipath detection and extraction. In the considerably shortened overall processing of Fig. 31b, such a modified FFT may lead to a noticeable reduction in processing time.

7.4 Potential Practical Application on HF Links

The potential utility of multipath processing using the cepstrum depends on a variety of factors. Assuming that tests of the type suggested in Sec. 7.2 turn out favorably and a suitable means for identifying the sign of τ is available, then there are the following to be considered:

- a) Expected rate of variation in α, τ
- b) How many multipath components are likely to be present, with what distribution of strengths
- c) How much improvement in the signal-to-interference ratio is required so that the data modem produces an acceptable error rate
- d) Signal-to-noise ratio at the receiver.

These parameters determine the accuracy with which the multipath parameters must be determined, at what rate they have to be measured, and whether averaging over several measurements can be used.

Another important question which has not yet been considered is the precision required in the FFT and other processing steps, for satisfactory performance. A preliminary examination of FFT precision, however, can be based on available literature. Thus Weinstein [7] derived the following estimate of the coefficient quantization effect at the output of a radix-2 FFT:

$$\frac{\sigma_E^2}{\sigma_Y^2} = (v/6)2^{-2q}, \quad (7-4)$$

- where
- σ_E^2 = error variance
 - σ_Y^2 = output signal variance
 - v = $\log_2 N$
 - q = number of binary digits in the mantissa.

An expression for the fixed-point roundoff error is also obtained in [7], namely,

$$\frac{\sigma_E^2}{\sigma_Y^2} = \frac{(5/3)N2^{-2q}}{\sigma_x^2} \quad (7-5)$$

where σ_x^2 = input signal variance.

Suppose the combined effects of coefficient quantization and roundoff are to result in an output noise-to-signal ratio of no more than -40 db, for $N = 512$. The input signal variance may be set at $\sigma_x^2 = 1/16$ in order to avoid overflow, since fixed-point arithmetic is assumed. If equal contributions to the output noise from coefficient quantization and from roundoff is assumed, then $\sigma_E^2/\sigma_Y^2 = -43$ db is substituted in both (7-4) and (7-5). This results in a requirement of 9 binary digits (including sign) for coefficient storage, and 16 binary digits (including sign) for arithmetic units. This is nominal for existing FFT processors [8].

Of course, once a specific FFT processor design is under consideration, a detailed error analysis, similar to [9], can be carried out.

Combining some of the suggestions in Sec. 7.2 and 7.3, a practical multipath canceller might take the form of specialized hardware for estimating multipath data (Fig. 31 b), the output of which is used to periodically update the parameters of a recursive canceller (Fig. 30). This canceller operates on the received signal in real time, or with a fixed delay to compensate for the processing time. In such an arrangement, processing speed can be sacrificed, as long as the multipath structure does not change too rapidly.

References

1. A.V. Oppenheim, R.W. Schafer, and T.G. Stockham, "Nonlinear Filtering of Multiplied and Convolved Signals", Proc. IEEE 56 (8) 1264-1291. August 1968.
2. R.P. Bogert, M.J. Healy, and J.W. Tukey, "The Quefrency Alalysis of Time Series for Echoes: Cepstrum, Pseudo-Autocovariance, Cross-Cepstrum and Saphe Cracking" Chapter 15 in Time Series Analysis, M. Rosenblatt ed., John Wiley and Sons, New York, 1963.
3. A.V. Oppenheim, "Superposition in a Class of Nonlinear Systems", Tech. Report 432, Res. Lab. of Electronics, M.I.T., Cambridge, Mass. March 31, 1965.
4. M.L. Uhrich, "Fast Fourier Transforms Without Sorting" IEEE Trans. AU-17 (2) 170-172. June 1969.
5. H. Schwarzlander, "Nonlinear Signal Processing - Progress Report No. 2" Tech. Memo. TM-71-1 Electrical Engg. Dept., Syracuse University, Syracuse, N.Y. March 1971.
6. M.J. DiToro, "Communication in Time-Frequency Spread Media Using Adaptive Equalization", Proc. IEEE 56 (10) 1654-1679. Oct. 1968.
7. C.J. Weinstein, "Quantization Effects in Digital Filters", Tech. Rept. 468, Lincoln Lab., M.I.T., Lexington, Mass. Nov. 21, 1969.
8. G.D. Bergland, "Fast Fourier Transform Hardware Implementations - A Survey", IEEE Trans. AU-17 (2) 109-119. June 1969.
9. R. Wasiewicz, "Quantization Error Analysis of an FFT-16 With Application to Matched Filtering of Linear-Frequency Modulated Radar Waveforms", M.S. Thesis, Syracuse University. January 1971.
10. H. Schwarzlander, "Nonlinear Signal Processing - Progress Report No. 1" Tech. Memo, TM-70-2 Electrical Engg. Dept., Syracuse University, Syracuse, N.Y. December 1970.